DOT HS 807 035
Final Report

August 1986

Preliminary Development -- Head-Neck Simulator

Volume II: Mathematical Simulations

Technical Report Documentation Page

1. Report No.	2. Government Accession No.	3. Recipient's Catalog No.
DOT HS 807 035		

4. Title and Subtitle

Preliminary Development of Head-Neck Simulator, V. 2.
VOLUME II: Mathematical Simulations

5. Report Date
August 1986

6. Performing Organization Code

8. Performing Organization Report No.
700560478-B

7. Author(s)
Hoen, T.G.M. and Wismans, J.S.H.M.

9. Performing Organization Name and Address
Research Institute for Road Vehicles TNO
Delft, The Netherlands

10. Work Unit No. (TRAIS)

11. Contract or Grant No.

12. Sponsoring Agency Name and Address
Vehicle Research and Test Center
National Highway Traffic Safety Admin.
400 7th Street, S.W.
Washington, D.C. 20590

13. Type of Report and Period Covered
Sept. 82 - Oct. 84
FINAL REPORT

14. Sponsoring Agency Code
Project SRL-59

15. Supplementary Notes

16. Abstract

This report documents the initial work of an ongoing research program of which the objective is to develop a head-neck simulator with omni-directional biofidelity. The report is composed of two volumes: VOLUME I: Analysis Volunteer Tests and VOLUME II: Mathematical Simulations.

In VOLUME I, a detailed analysis is presented of a large number of human volunteer tests conducted by the Naval Biodynamics Laboratory in New Orleans. These human subjects were exposed to frontal, lateral and oblique impacts with an impact severity up to 15 g and 17 m/s. This analysis results for each impact direction in a simple analog system that completely specifies the observed dynamical behavior.

VOLUME II documents the validation of the proposed analog systems and compares the behavior of the Part 572 and Hybrid III head-neck systems with the human volunteer behavior. it follows that both neck designs are stiffer than any of the volunteers in the impact ranges tested. Preliminary results are presented of computer aided design activities in order to improve existing designs in view of these new findings.

17. Key Words	18. Distribution Statement
Head-Neck Simulator MADYMO Part 572 Dummy Hybrid III Dummy Anthropomorphic Test Device	Document is available to the public from the National Technical Information Service, Springfield, VA 22161

19. Security Classif. (of this report)	20. Security Classif. (of this page)	21. No. of Pages	22. Price
Unclassified	Unclassified		

Form DOT F 1700.7 (8-72) Reproduction of completed page authorized

ABSTRACT

This report documents the work conducted in phase I of an ongoing research program of which the objective is to develop a head-neck simulator with omni-directional biofidelity. The report is composed of two volumes:
Vol. I : Analysis volunteer tests
Vol. II: Mathematical simulations

In Vol. I a detailed analysis is presented of a large number of human volunteer tests conducted by the Naval Biodynamics Laboratory in New Orleans. These human subjects were exposed to frontal, lateral and oblique impacts with an impact severity up to 15 g and 17 m/s. This analysis results for each impact direction in a simple analog system that completely specifies the observed dynamical behaviour.

Vol. II documents the validation of the proposed analog systems and compares the behaviour of the Part 572 and Hybrid III head-neck systems with the human volunteer behaviour. It follows that both neck designs are stiffer than any of the volunteers in the impact ranges tested. Preliminary results are presented of computer aided design activities in order to improve existing designs in view of these new findings.

TABLE OF CONTENTS

LIST OF TABLES

LIST OF FIGURES

CHAPTER 1

INTRODUCTION

1.1 Project description and objectives

The National Highway Traffic Safety Administration (NHTSA) has large quantities of test data on the head and neck response of human volunteer subjects in frontal, oblique and lateral sled tests. The Vehicle Research and Test Center (VRTC) will use these data for the development of an improved head-neck motion simulator. Where possible, these human test data will be augmented by data of human cadavers tested at exposure levels beyond those generally acceptable for human volunteers.

One or more candidate mechanical systems will be identified to reproduce observed head-neck motions. Currently identified models will form the basis for this analysis but the study will not necessarily be limited to such models. The performance of candidate mechanical neck simulators will be analyzed and optimized using mathematical model simulations resulting finally in design specification for an improved dummy neck.

This report presents the results of phase I of this ongoing research program. The report is composed of two volumes:

Volume I : Analysis volunteer tests

Volume II : Mathematical simulations.

In Vol. I an analysis is presented of a number of human volunteer tests in three different impact directions conducted at the Naval Biodynamics Laboratory (NBDL)*. This analysis results for each impact direction in an analog system that completely specifies the observed dynamical behaviour. Vol. II documents the validation of the proposed analog systems by means of mathematical simulations and presents a number of preliminary computer aided design activities carried out in order to improve existing dummy necks in view of these new findings.

---

* NBDL: Naval Biodynamics Laboratory in New Orleans, previously Naval Aerospace Medical Research Laboratory Detachment (NAMRLD)

1.2 Summary research program: mathematical simulations

During this study numerous mathematical simulations were conducted. The most interesting ones will be summarized here. These calculations were conducted with the MADYMO Crash Victim Simulation program package (1).

Chapter 2 presents simulations performed for validation of the analog systems proposed in Vol. I. Three 2-pivot linkage systems have been proposed in Vol. I: one for the behaviour in frontal impacts, one for oblique impacts and one for lateral ones. Simulations will be presented here for all three impact directions. Results of some of the parameter variations conducted in order to improve the insight in the system's behaviour will also be presented in this chapter.

Chapter 3 deals with a model for the Part 572 dummy head-neck assembly in frontal impacts. The neck section of this model consists of 7 segments. Model results will be compared with the Part 572 pendulum calibration test and with sled tests.

In chapter 4 the behaviour of the Part 572 and Hybrid III dummy head-neck assemblies will be compared with the human volunteer behaviour. Significant differences between dummy and volunteer can be observed. The model of the Part 572 dummy presented in chapter 3 will be used to analyze the effect of possible design changes.

The major findings of these model simulations will be summarized and discussed in chapter 5. Based on these findings recommendations are made for improvement of the procedure used to analyze human volunteer test data. Also a preliminary design recommendation will be made for a dummy neck with frontal biofidelity.

CHAPTER 2

SIMULATION OF THE HEAD-NECK MOTION OF HUMAN VOLUNTEERS BY A TWO-PIVOT MECHANISM

2.1 Introduction

In this chapter the validation of the system for the human head-neck behaviour proposed in Vol. I will be presented. The analysis is limited to the loading phase of the motion. A summary of the system parameters of the two-pivot mechanism specified in Vol. I will be presented in section 2.2, while the representation of this mechanism in the MADYMO Crash Victim Simulator is described in section 2.3. In section 2.4 results of the validation efforts are presented. An analysis of deviations between model and experiments is given in section 2.5. Using the model, the effect of a number of parameter variations was evaluated. Some of the most interesting variations will be presented in section 2.6.

2.2 Summary of the system parameters provided in Vol. I

Table 1 summarizes the most important linkage parameters of the analog systems proposed in Vol. I (Fig. 1). The orientation of the head principal axes and the location of occipital condyles and center of gravity will be specified in agreement with the assumptions made in Vol. I:

- the angle between principal z-axis and head anatomical z-axis is -36° (principal z-axis rotated backward)
- occipital condyles relative to head anatomical coordinate system:
  x = -1.1 cm y = 0 cm z = -2.6 cm
- center of gravity relative to head anatomical coordinate system:
  x = 1.2 cm y = 0 cm z = 2.9 cm

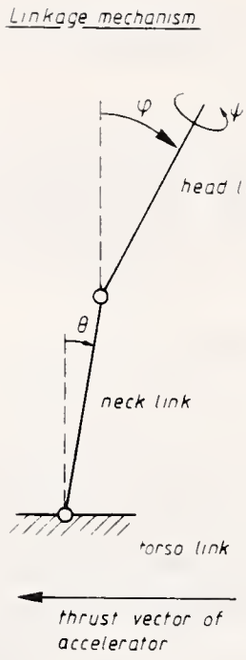

Fig. 1 Two-pivot model for the human head-neck system.

Fig. 2 illustrates the location of the head center of gravity relative to a coordinate system oriented along the principal axes with the origin near the occipital condyles.

The mass and moments of inertia of the head in the model will be based on estimated values for subjects H00083 and H00093 (see Table 6, Vol. I). The mean value of these data (including instrumentation) is used as model input and is incorporated in Table 1.

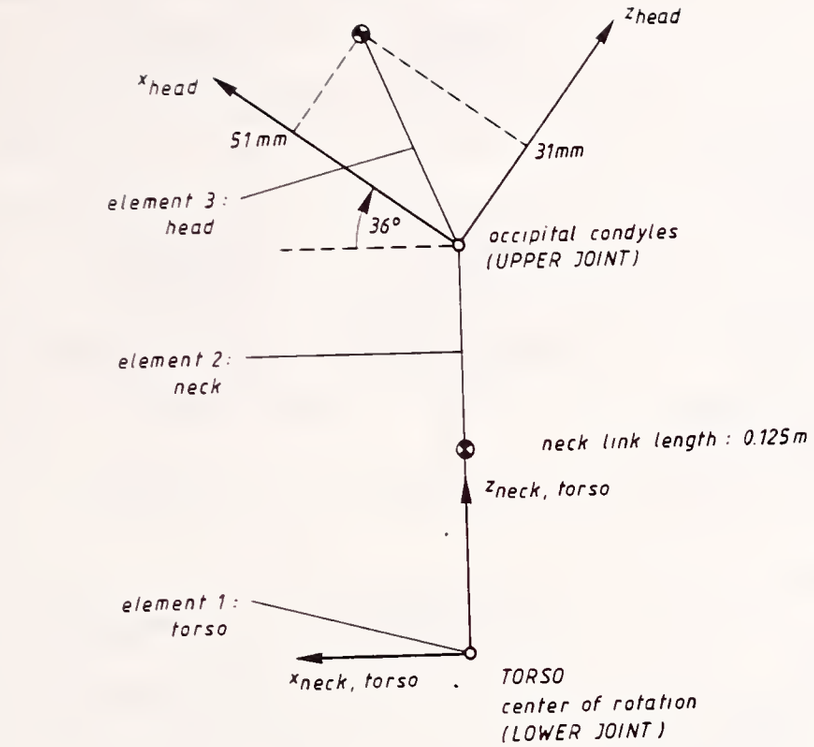

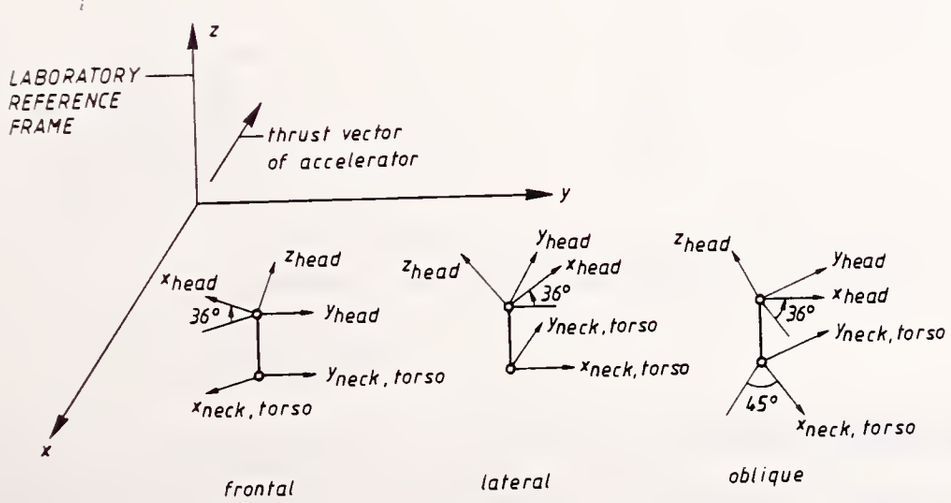

Fig. 2 Orientation of coordinate systems.

Table 1 Linkage parameters for the loading phase based on 30 impact tests with two subjects (H00083 and H00093).

Parameter	Frontal direction	Lateral direction	Oblique direction
Geometrical parameters			
upper pivot location	occipital condyles	occipital condyles	occipital condyles
link length	0.125 m	0.125 m	0.125 m
lower pivot location	see table 8 (Vol. I)	see table 8 (Vol. I)	see table 8 (Vol. I)
initial head link flexion	0	0	0
initial head link torsion	0	0	0
initial neck link rotation	14 deg.	5 deg.	10 deg.
Joint parameters			
lower pivot linear stiffness	1.25 Nm/deg.	1.5 Nm/deg.	1.25 Nm/deg.
upper pivot linear torsion stiffness	-	0.25 Nm/deg.	0.5 Nm/deg.
upper pivot free range of motion in the plane of impact*	25°	10°	20°
Mass distribution			
head center of gravity		see fig. 2	
mass		4.28 kg	
I_{xx}		0.0230 kg.m^2	
I_{yy}		0.0238 kg.m^2	
I_{zz}		0.0124 kg.m^2	

* Joint is locked if maximum excursion is reached.

2.3 MADYMO model set-up

The model consists of three elements (torso, neck and head) connected by two ball and socket joints. The element and absolute coordinate systems are illustrated in Figure 2. For the lateral and oblique simulations the torso, neck and head links are rotated 90 and 45 degrees, respectively, about the z-axis of the absolute (laboratory) reference frame. The initial orientation of the segments in the present MADYMO version (i.e. version 3) has to be specified by so-called Bryant angles. For the lateral and oblique simulations these angles were obtained by a pre-processing program.

For the simulations presented here a new joint model was developed: the flexion-torsion joint model (Fig. 3). Consider the joint between element i and element j. In both elements vectors $\underline{t}$ and $\underline{f}$ are defined. By means of these vectors it is possible to specify two rotations α and β, respectively. The rotation α is the angle between the vectors $\underline{t}_i$ and $\underline{t}_j$ and is called the flexion angle. This angle is defined in the interval from 0 to 180 degrees. As a consequence of the rotation α the vector $\underline{f}_i$ takes a new position $\underline{f}_j'$. The angle β is defined as the rotation around the $\underline{t}_j$-axis, which transforms $\underline{f}_j'$ into $\underline{f}_j$. This angle is called the torsion angle and is defined from -180 to + 180 degrees. In this way it is possible to specify two torques, i.e. a flexion and a torsion torque.

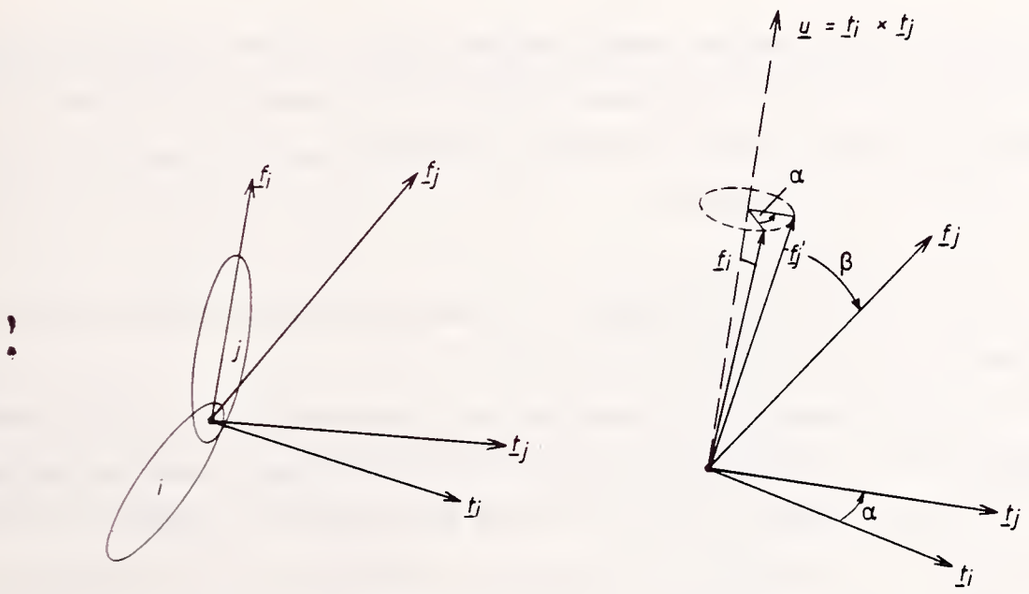

Fig. 3 Flexion-torsion model.

Fig. 4 shows the $\underline{t}$ and $\underline{f}$ vectors used for the human head-neck system. A more detailed description of this joint model is presented in Appendix A.

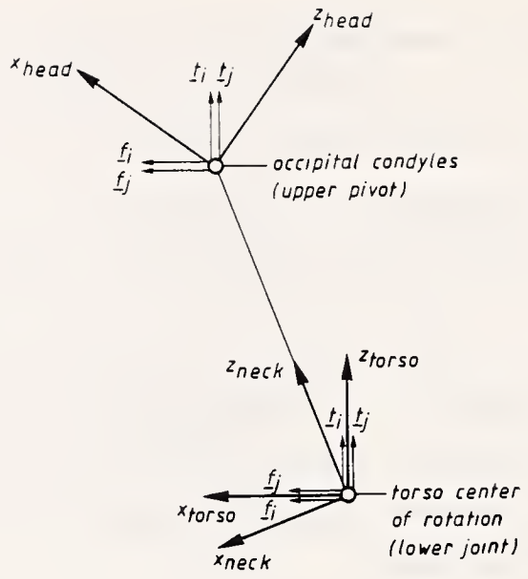

Fig. 4 Definitions of the $\underline{t}$ and $\underline{f}$ vectors in the two-pivot model.

This new joint model can be used for the lower pivot using the lower pivot linear flexion stiffness specified in Table 1 as torque-flexion characteristic. Torsion in the lower pivot will be suppressed since the upper pivot already allows a torsion motion.

For the upper pivot the situation is more complicated due to the required locking behaviour. For the loading phase of this joint, i.e. the phase where the angle α increases, in a standard way the torque-rotation function as illustrated in Fig. 5a can be prescribed. The free range of motion α_o is different for each impact direction as illustrated in Table 1. The joint stop stiffness is arbitrarily selected as 500 Nm/rad. For unloading (i.e. α becomes smaller) the same characteristic can be used until α_o is reached. If α becomes smaller than α_o the original torque-rotation relation has to be adjusted in order to obtain the locking effect. This new characteristic is illustrated in Fig. 5b. In some of the mathematical simulations, which will be treated later, it was found that the joint stop of the upper pivot was not reached and consequently the locking mechanism was not activated. Due to this the joint model was modified in such a way that the locking mechanism is activated even if α doesn't reach to α_o-value. Torsion characteristics for the upper pivot are defined according to Table 1.

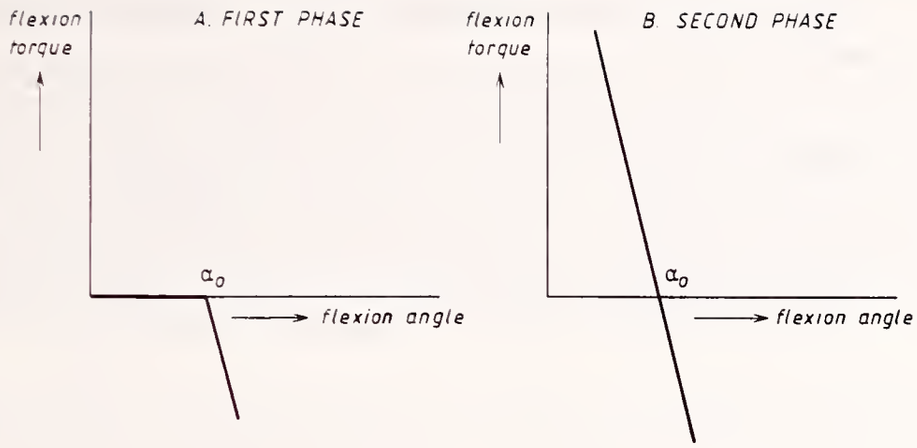

Fig. 5 Flexion characteristic of the upper pivot.

For the flexion motion of the upper pivot damping will be specified which is activated in the joint stop. To investigate the influence of this damping two simulations of a frontal volunteer test (representative for LX3544, LX3548 and LX3550) were conducted:

- DAMP 1: undamped model
- DAMP 2: model with a damping coefficient of 1 Nms/rad.

Significant oscillations are present in the accelerations in case of absence of damping (Fig. 6). The effect of this damping on the rotations of the neck and head element, however, is small.

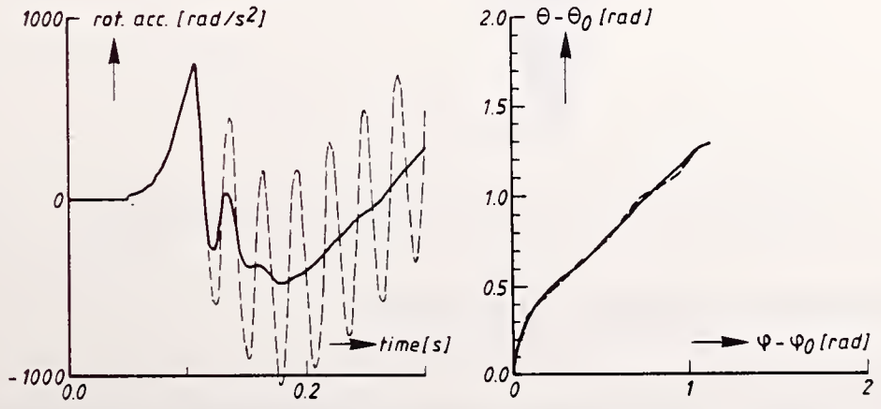

Fig. 6 Model results from a simulation of a frontal volunteer test for an undamped (DAMP1) and a damped upper pivot joint (DAMP2).

In the flexion-torsion joint model a third direction of motion can be distinguished, namely perpendicular to the flexion direction (Fig. 7). Mathematical simulations showed, that after the locking mechanism is activated, the $\underline{t}_j$ vectors tended to slide away in the third motion direction along a cone (Fig. 7). As a consequence, out of plane motion will occur and the $\underline{t}_j$ vector can move to the other side of the cone dependent on the loads acting on the head-neck system. To prevent this undesirable motion, linear damping was specified in this third direction. For the simulations described in this chapter a damping coefficient of 10 Nms/rad is selected.

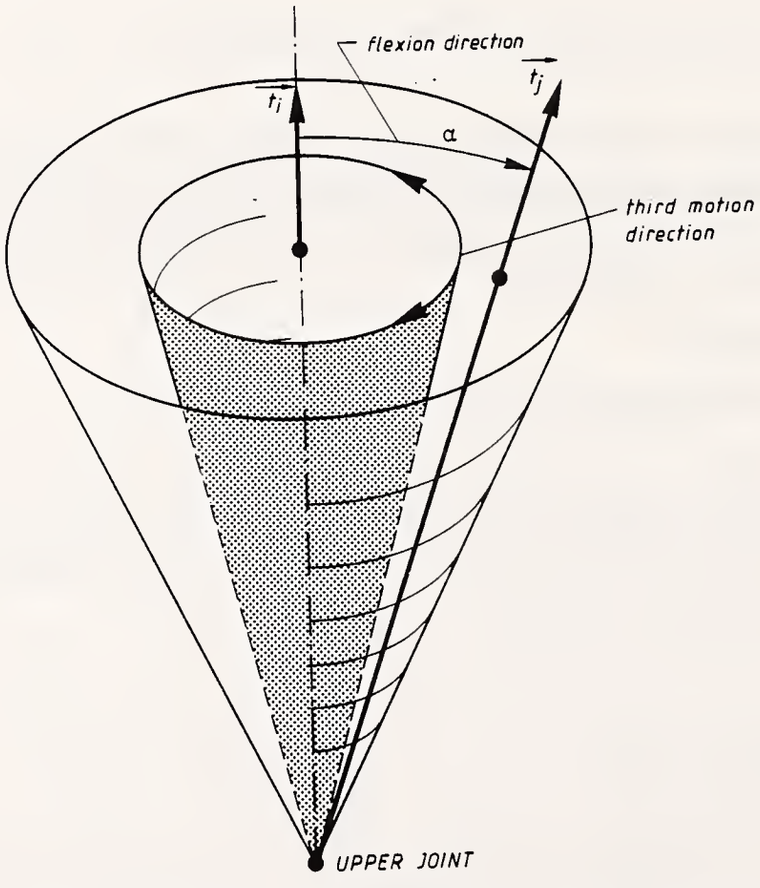

Fig. 7 Third motion direction in the flexion-model.

2.4 Validation of the two pivot model

The model runs for the three impact directions with data-sets as described in the preceding sections will be called the reference simulations. In Appendix B the input data-sets are presented. These simulations will be compared with a set of tests under similar conditions:

- frontal impacts: LX3544, LX3548 and LX3550
- lateral impacts: LX1831, LX2013 and LX2355
- oblique impacts: LX3133, LX3153, LX3122 and LX3158.

All these tests are of a moderate severity. The test conditions are presented in Table 3 in Vol. I. As part of the sensitivity study (section 2.6), the most severe volunteer test (test LX3616) in the present data base will be simulated separately. An approximation for the T1 acceleration measured in the volunteer tests will be used as model input (Fig. 8).

The following output parameters will be used for model validation:
- head torsion and neck link rotation as function of the head flexion,
- head and neck rotations as functions of time as defined in Fig. 1,
- linear accelerations of the head anatomical origin with respect to the laboratory reference frame as function of time,
- head angular accelerations as function of time.

Model results (REF1) and test results for the frontal impact situation are presented in Figs. 9-10. Fig. 9 shows that head and neck rotation functions are predicted very well by the model. A small difference can be observed for the head flexion ϕ and the corresponding angular accelerations, which start too early in the model. Due to this the maximum relative angle between the head and neck element is only 16 degrees, while the volunteer tests showed an average value of 25 degrees.

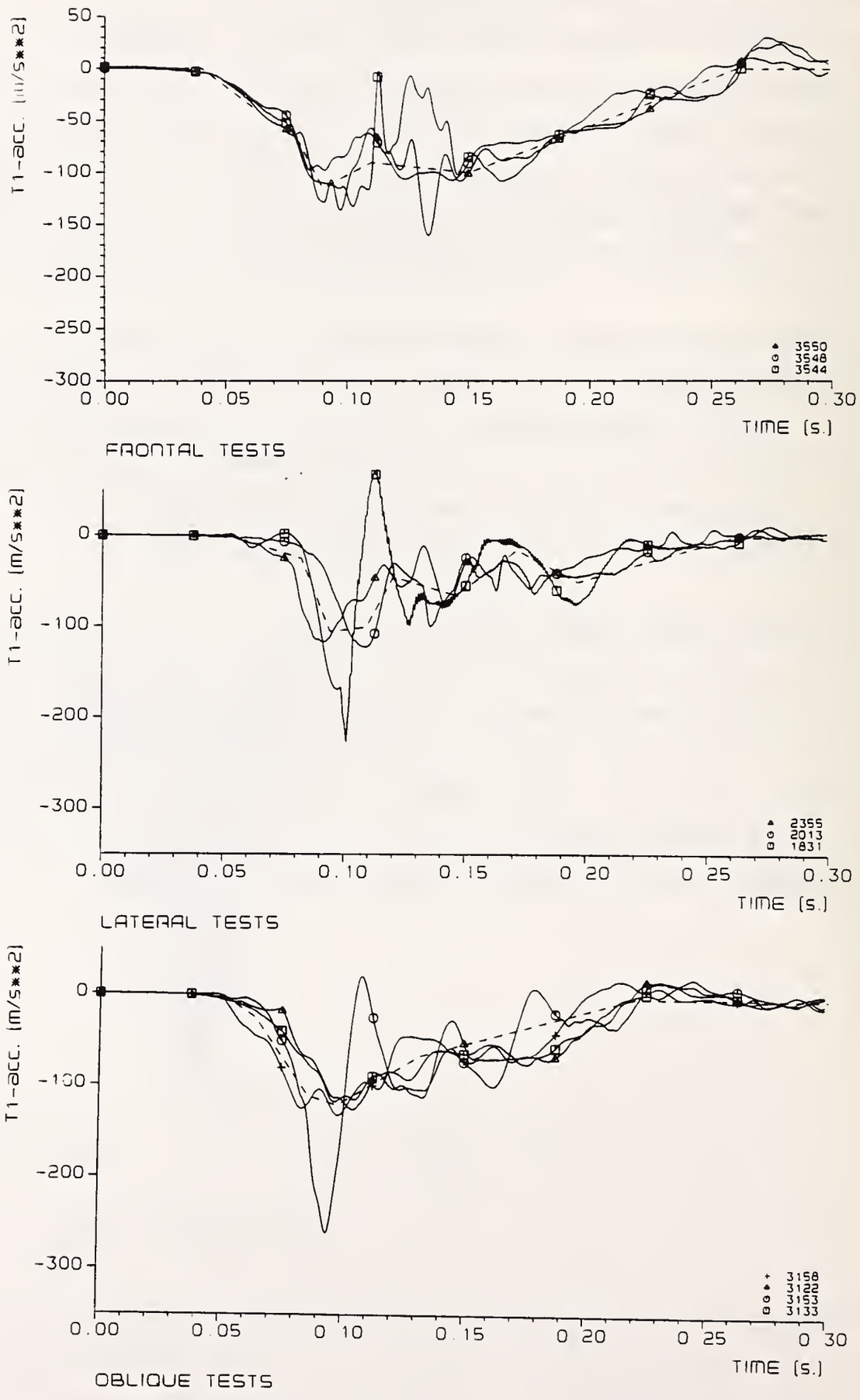

Fig. 8 T1 accelerations and model input in frontal, lateral and oblique direction.

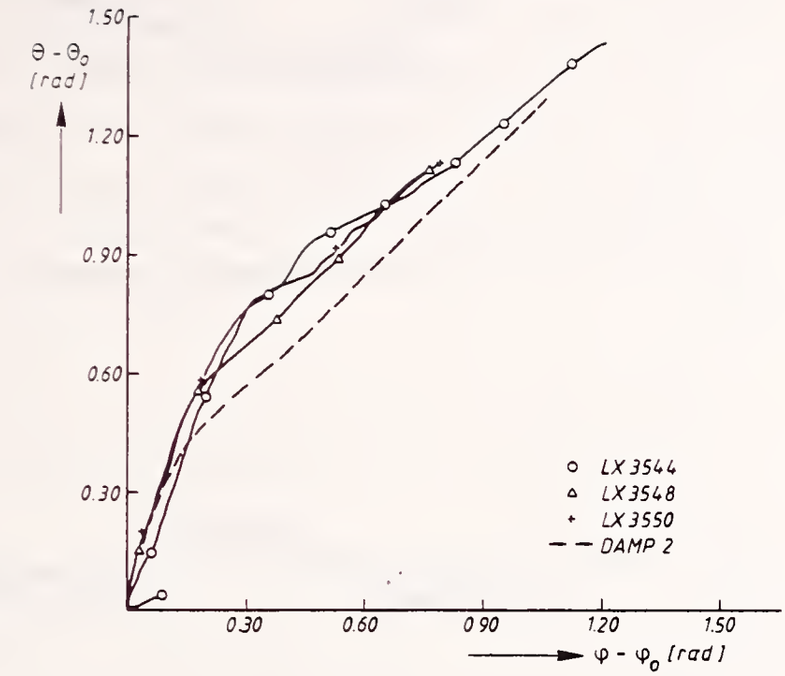

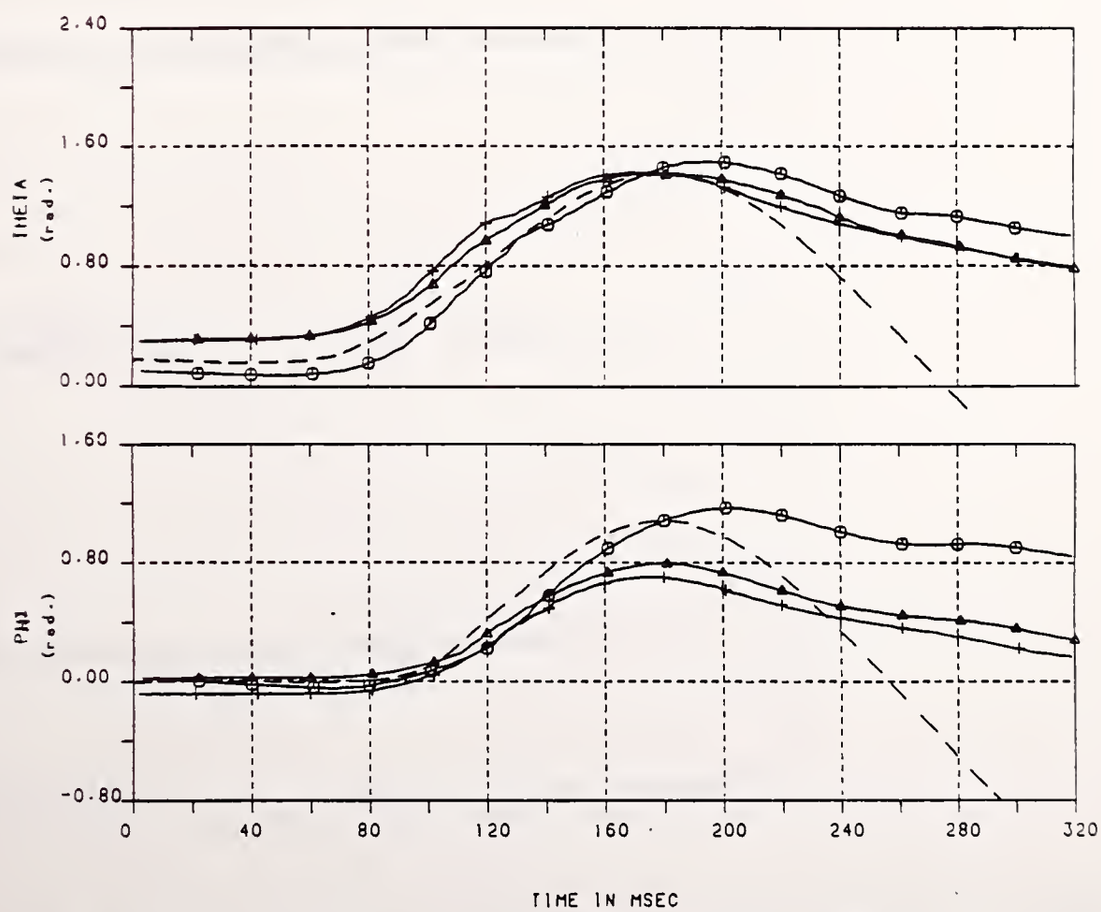

Fig. 9 Rotations for the frontal volunteer tests and the reference model run (REF1=DAMP2).

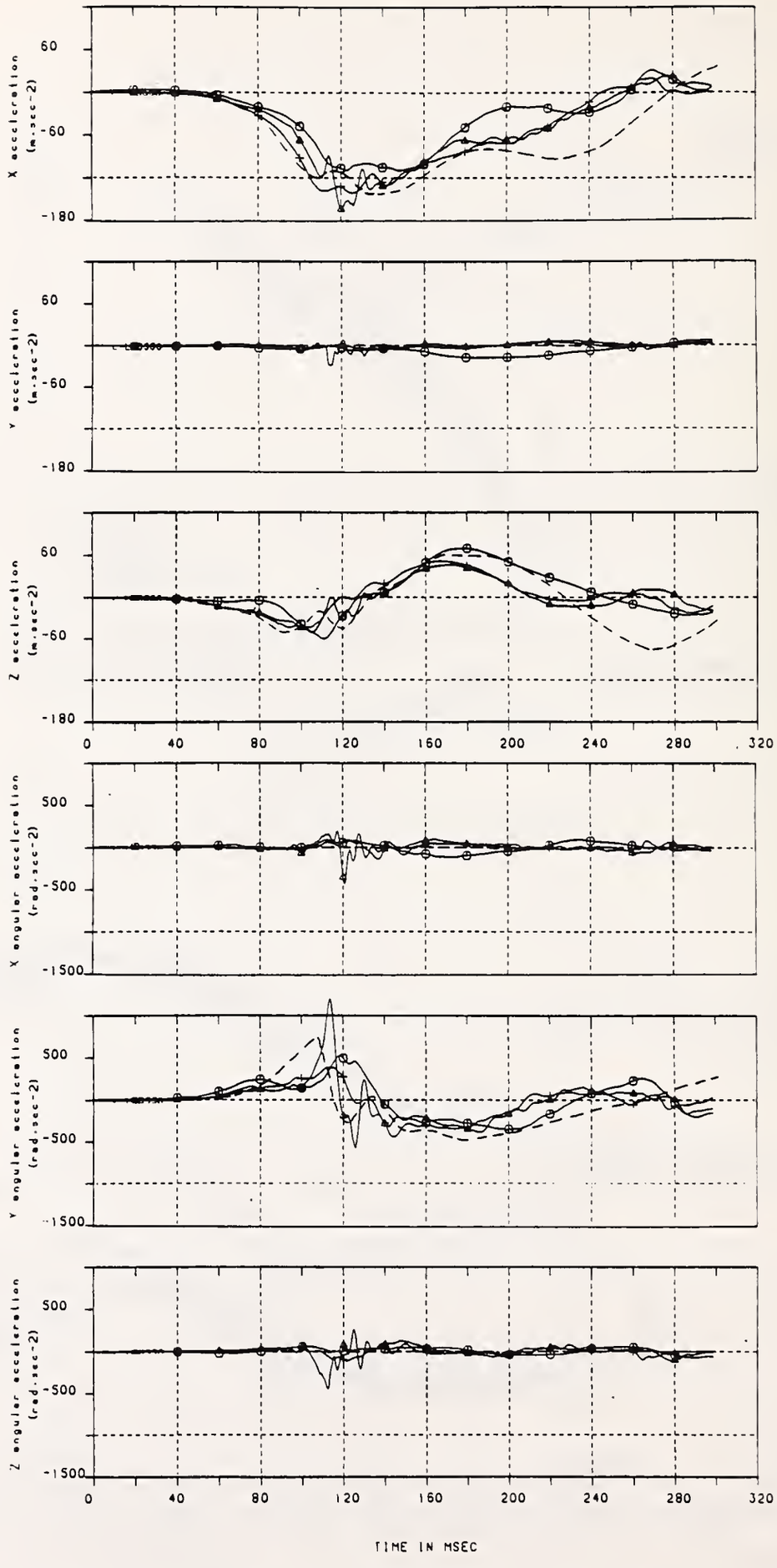

Fig. 10 Linear accelerations of the anatomical origin in laboratory directions and head angular accelerations for the frontal volunteer tests and the reference model run (REF1=DAMP2).

Results of the simulation (REF2) for the lateral volunteer tests appear to be slightly closer to the volunteer tests than the results of the frontal test simulation (Figs. 11 and 12). The same holds for the simulation of the oblique tests (REF3) with one exception: the head torsion ψ is predicted by the model is too small (Figs. 13 and 14). The maximum relative flexion angle in the upper pivot appears to be predicted adequately by both the lateral and oblique model set-ups (Figs. 11 and 13).

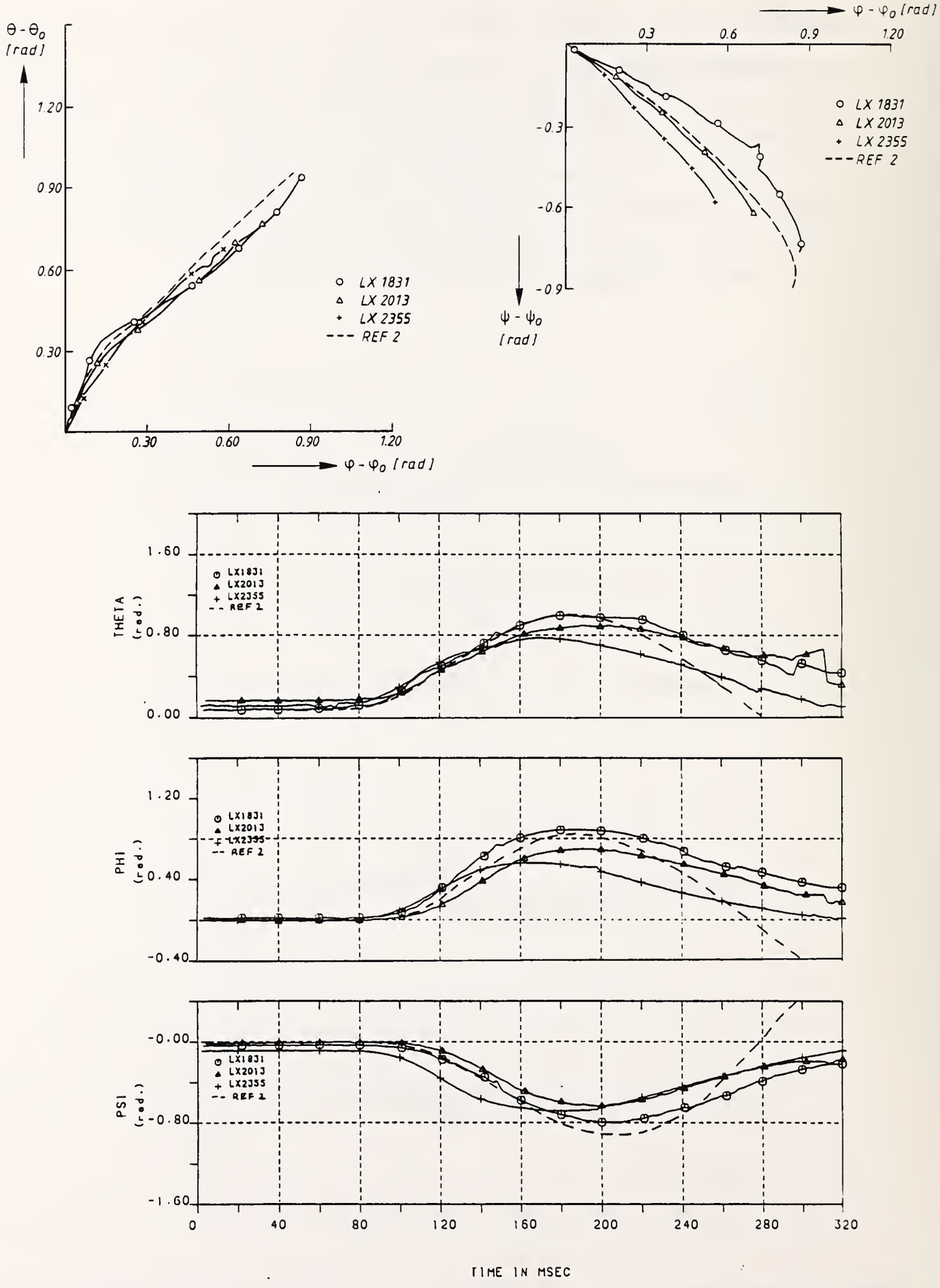

Fig. 11 Rotations for the lateral volunteer tests and the reference model run (REF2).

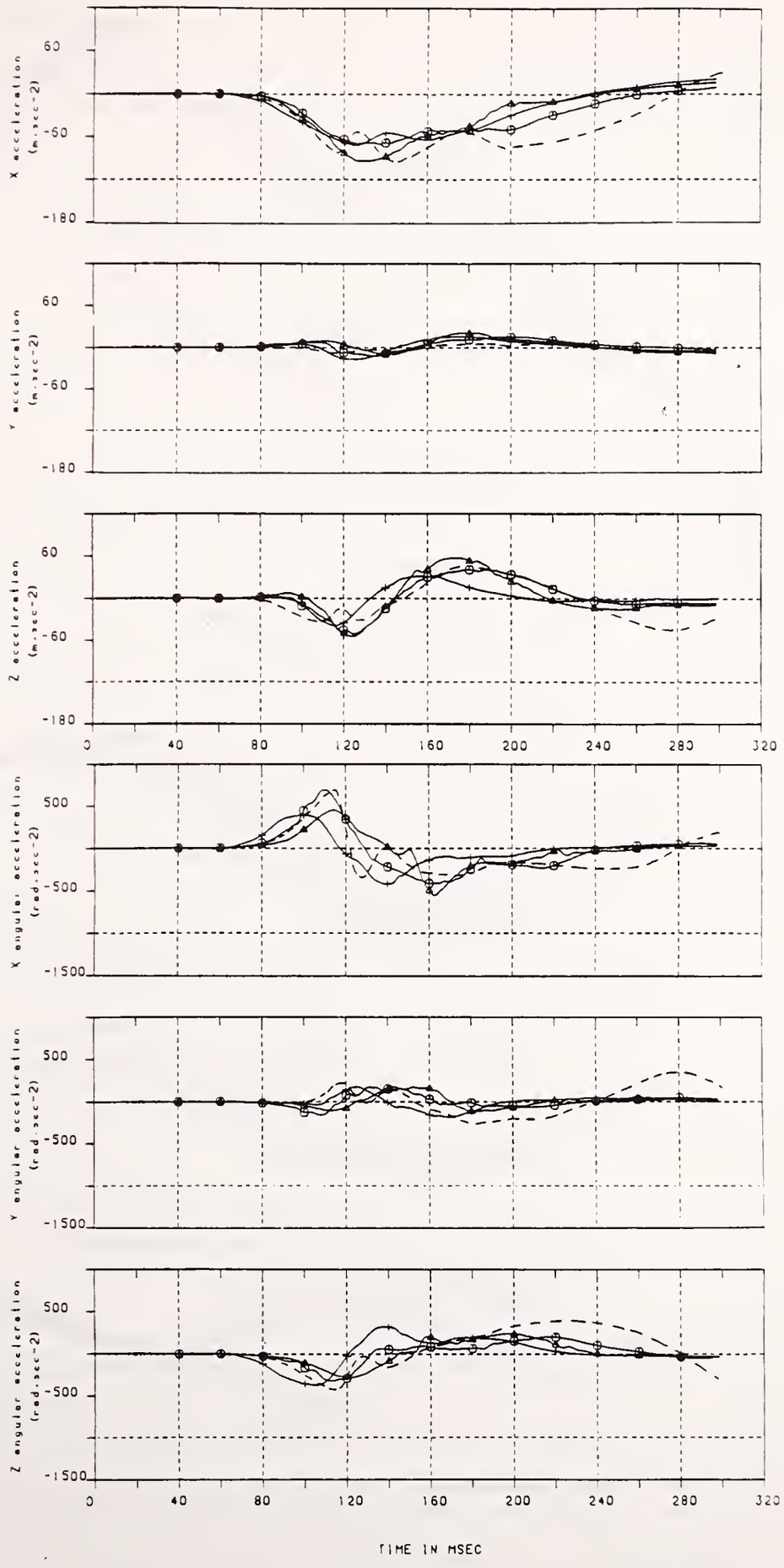

Fig. 12 Linear accelerations for the anatomical origin in laboratory directions and head angular accelerations of the lateral volunteer tests and the reference model run (REF2).

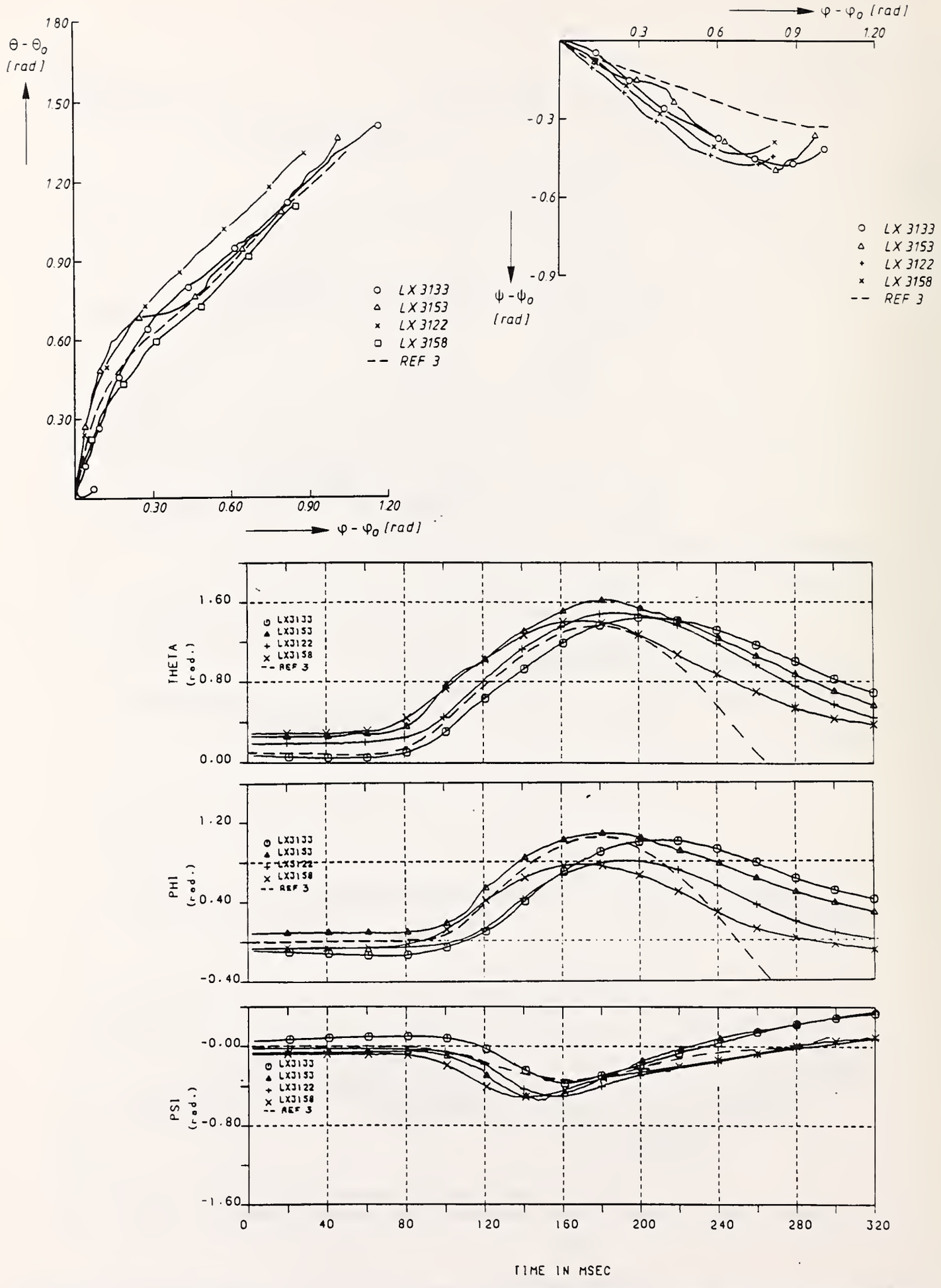

Fig. 13 Rotations for the oblique volunteer tests and the reference model run (REF3).

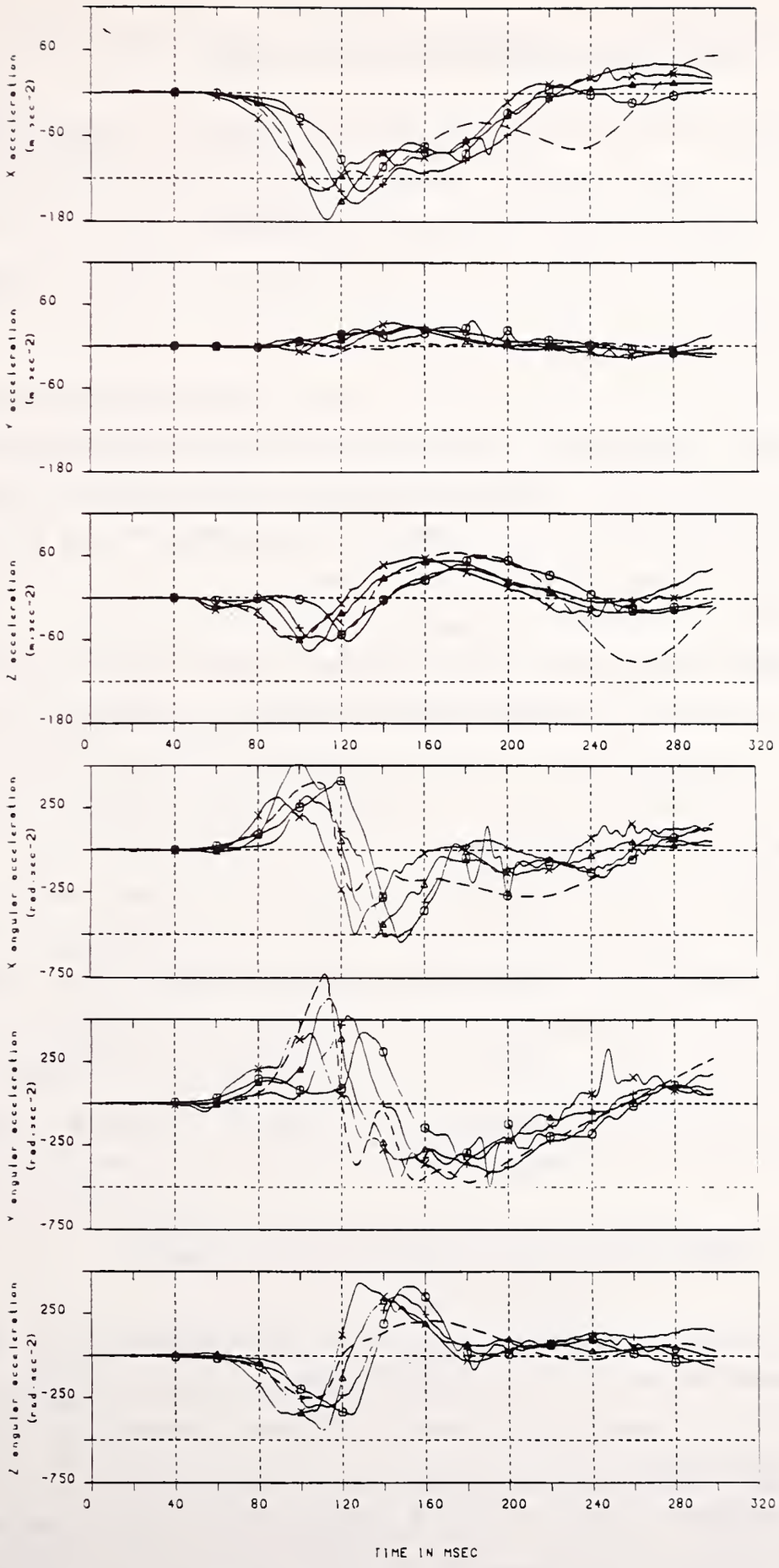

Fig. 14 Linear accelerations of the anatomical origin in laboratory directions and head angular accelerations for the oblique volunteer tests and the reference model run (REF3).

2.5 Conclusions from the validation study

The preceding simulations show two significant deficiencies in the model:
- the initial maximum relative upper pivot rotation in the impact plane is too small in case of frontal impacts,
- the head torsion β is not predicted well by the model in case of oblique impacts.

For the first deficiency the following explanation can be given: the initial joint characteristic of the lower pivot is expected to have a dominant influence on the initial relative rotation in the upper pivot. The joint characteristics used as model input for the lower pivot are based on estimations from the loads calculated with respect to T1 rather than the torso center of rotation (chapter 6 of Vol. I). As a consequence the selected joint characteristic for the lower pivot might not be completely correct. The influence of this stiffness will be illustrated in section 2.6.2.

The second deficiency is probably caused by the limited accuracy of the graphical technique used for the estimation of the upper pivot torsion stiffness. The effect of a different upper torsion stiffness will be illustrated in section 2.6.4. The different ways in which the head torsion is specified in model and volunteer tests could also contribute to the observed differences. For the volunteer tests, head torsion is derived from the third Euler angle. In the model, the torsion angle is determined according to the equations presented in section 2.3. The possible influence of this is not clear yet and is subject to further study.

2.6 Sensitivity study with the two-pivot model

A number of parameter variations were conducted in order to get a better understanding of the system behaviour and to explain differences between model and experiment. Some of the most interesting variations will be considered here:
- the model behaviour for a single severe test using subject specific data (2.6.1),
- the effect of lower pivot stiffness (section 2.6.2),

- the effect of the absence of a locking mechanism in the upper pivot (section 2.6.3),
- the effect of the torsion stiffness in the upper pivot (section 2.6.4).

2.6.1 Simulation of a single severe test using subject specific data

Simulations were conducted to evaluate the model validity for a higher impact severity and to analyse the effect of subject specific input data. Two simulations will be presented here:

- SEN1: simulation of the most severe volunteer test (subject H00093 in test LX3616) using subject specific data (see Table 2),
- SEN2: simulation of the most severe volunteer test using the reference data set.

In both simulations the initial head and neck link position was based on the actual position in the human volunteer test (see Table 2).

Table 2 Differences in system parameters relative to the reference simulation in simulations SEN1 and SEN2.

Parameter	SEN1	SEN2
- initial head link flexion in plane of impact	-12 [deg]	-12 [deg]
- initial neck link rotation in plane of impact	20 [deg]	20 [deg]
- lower pivot linear flexion stiffness	1.88 [Nm/deg]	
- head mass	4.03 [kg]	
- moments of inertia of the head:		
I_{xx}	0.0209	
I_{yy}	0.0215 [kg.m^2]	
I_{zz}	0.0110	

Fig. 15 shows the T1 acceleration of test LX3616 together with the model input. Model and test results are presented in Figs. 16 and 17. Both simulations appear to predict the results of this more severe test situation quite realistically. Fig. 16 shows that the model with the subject specific data performs slightly better than the model with the average linkage parameters.

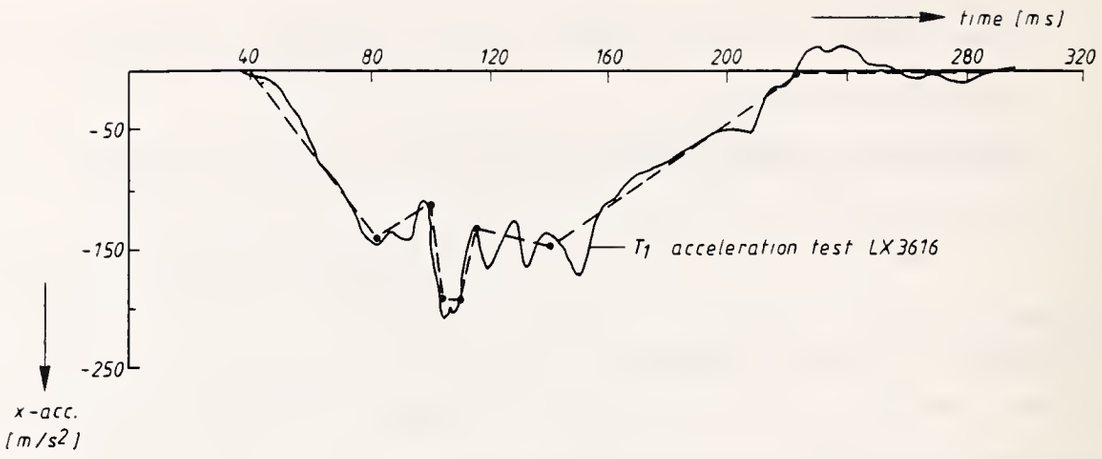

Fig. 15 T1 acceleration for the most severe volunteer test (LX3616) and model input.

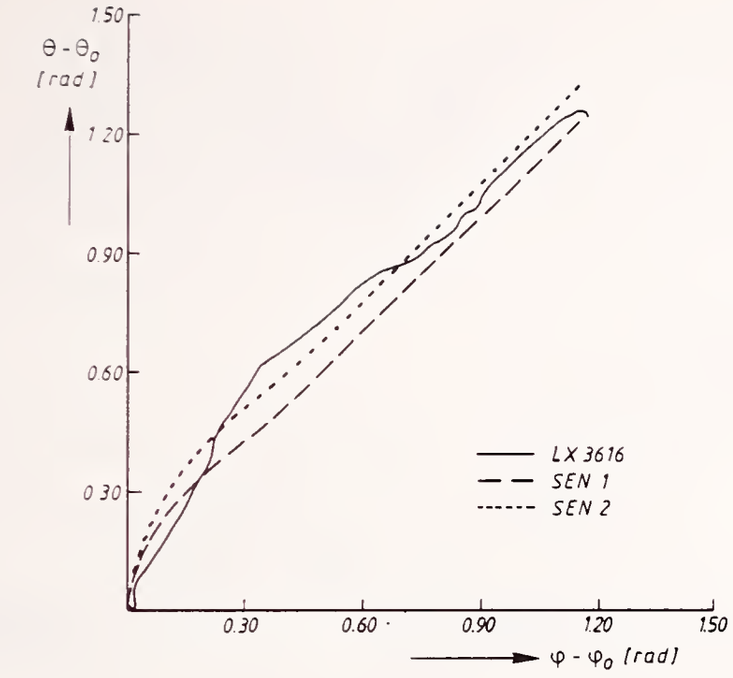

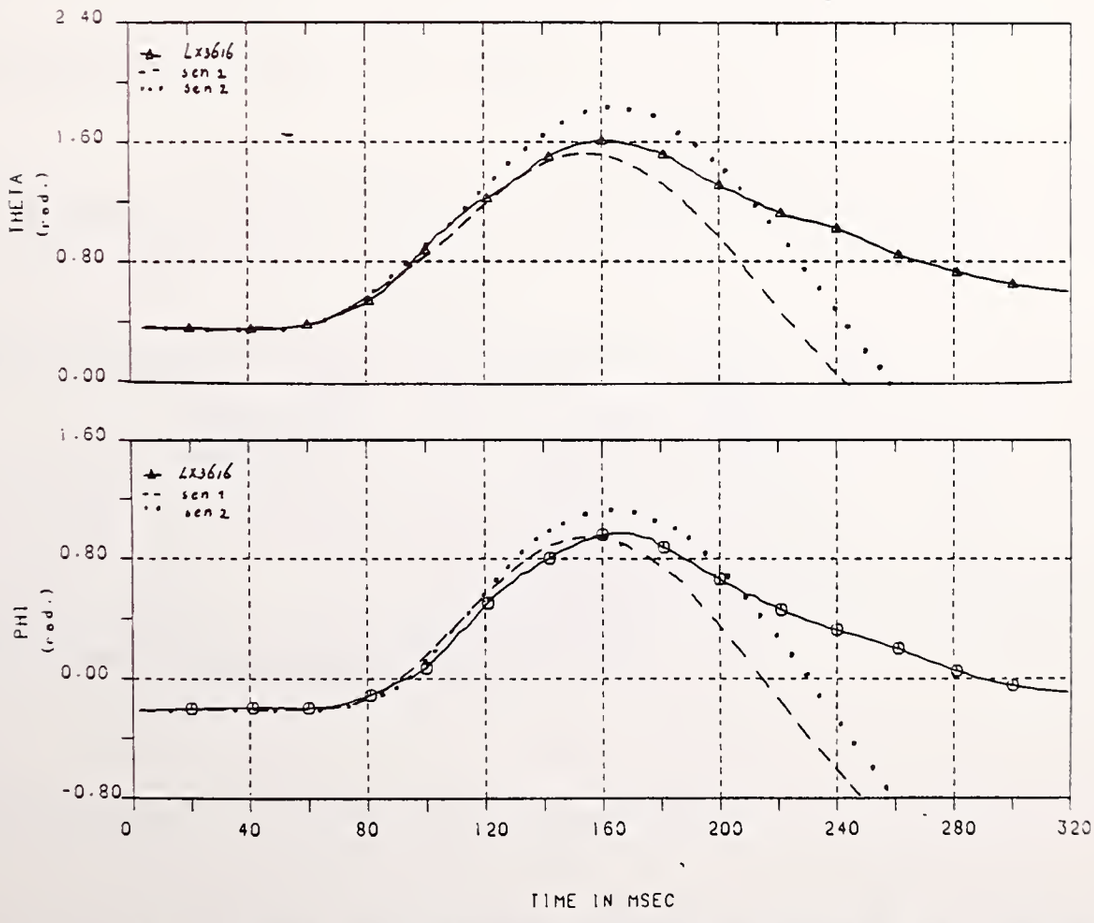

Fig. 16 Rotations for the most severe frontal volunteer test and model runs (SEN1 and SEN2).

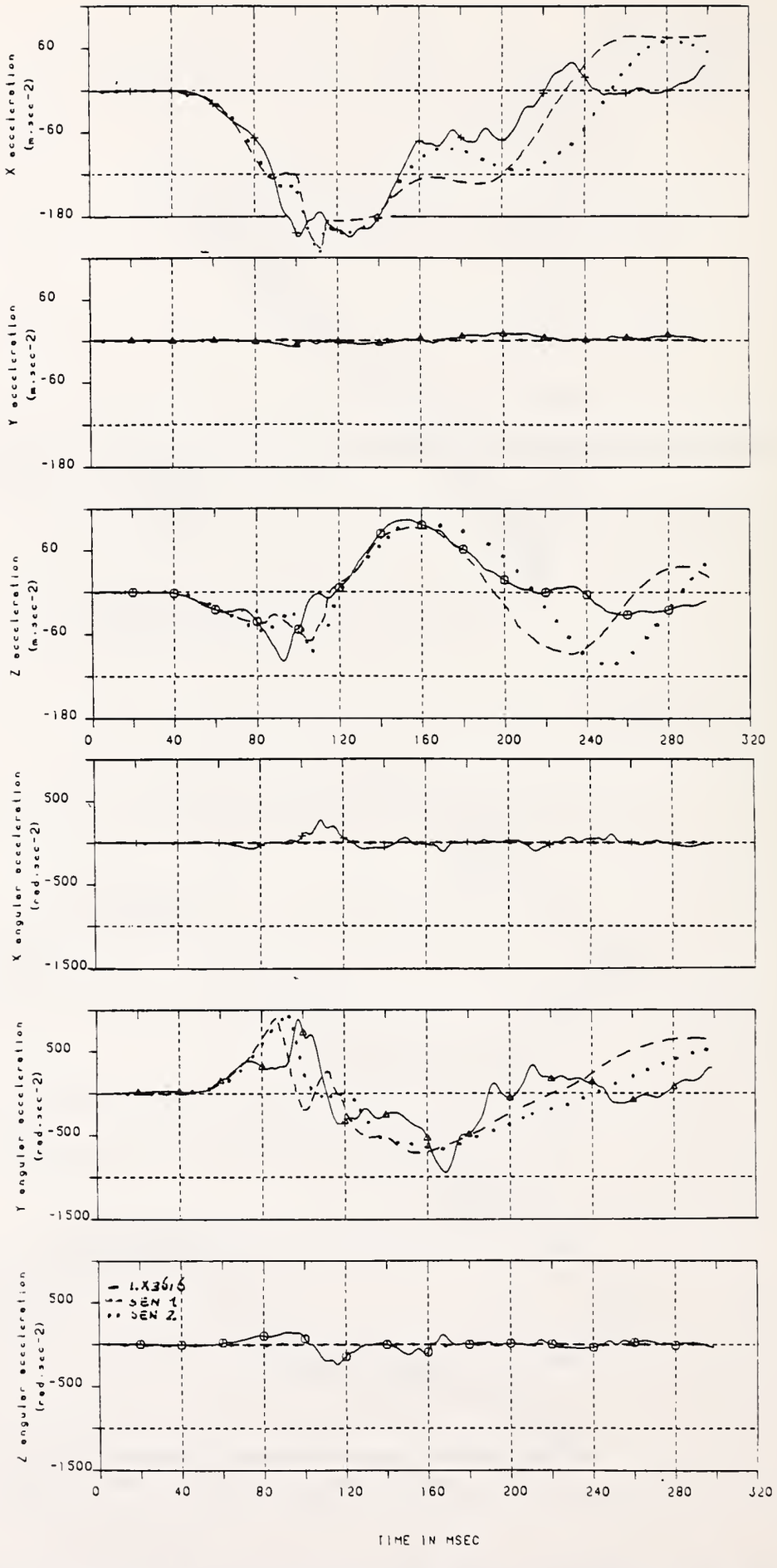

Fig. 17 Linear accelerations of the anatomical origin in laboratory directions and head angular accelerations for the most severe frontal volunteer test and model runs (SEN1 and SEN2).

2.6.2 The effect of the flexion characteristic of the lower pivot

Since the lower pivot stiffness was estimated rather than calculated, it was decided to perform a sensitivity study for the initial part of the torque-rotation characteristic (for larger rotation values the torque estimations are expected to be more accurate). One of the changes (SEN3) is shown in Fig. 18.

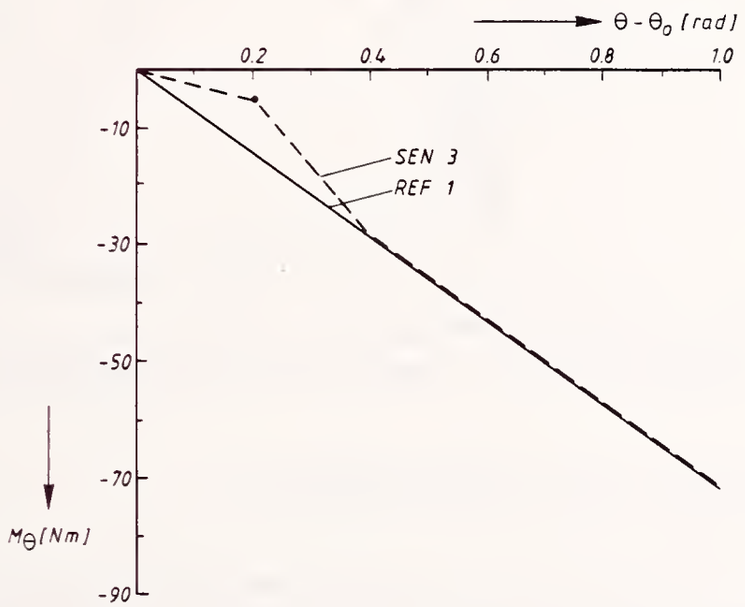

Fig. 18 Flexion characteristic of the lower joint in the reference model and in model SEN3.

From a comparison between Figs. 9 and 19 it can be concluded, that the model results are improved with respect to the maximum relative angle in the upper pivot. In these simulations, the relative angle reaches 23 degrees rather than the 16 degrees achieved in the reference simulation. Based on this relatively large influence it is recommended to calculate lower neck torques directly at the torso center of rotation rather than at T1. Other model results were hardly effected by this variation.

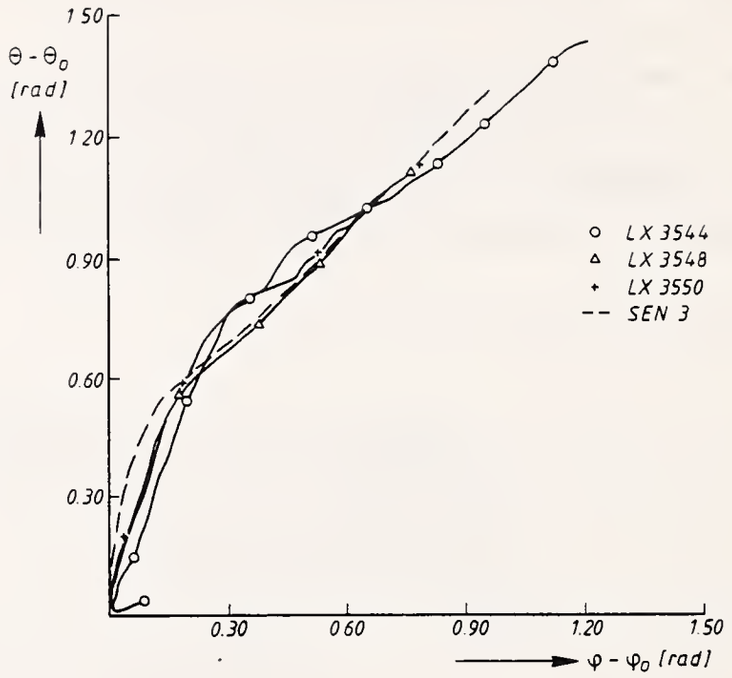

Fig. 19 Rotations for the frontal volunteer tests and the model run with a changed flexion characteristic of the lower joint (SEN3).

2.6.3 The effect of the locking mechanism

One of the most interesting findings from the analysis of the volunteer test was the existence of a so-called locking mechanism in the upper neck region. This mechanism, most likely due to muscle activity, was represented in the model by a relatively stiff torque-rotation characteristic of 500 Nm/rad (joint stop), which is activated as soon as the upper pivot reaches the locking or maximum position. In tests with human cadavers (no muscle activity) or for much higher impact levels this locking mechanism might be partly or completely absent. The possible effect of this is simulated by specifying a much lower locking stiffness (SEN4: 50 Nm/rad rather than 500 Nm/rad) and is illustrated in Fig. 20. From this figure it can be concluded that the neck rotation θ slightly decreases whereas the head rotation ϕ strongly increases compared to the reference simulation (Fig. 9). In other words, if the locking mechanism is absent the head will tip over.

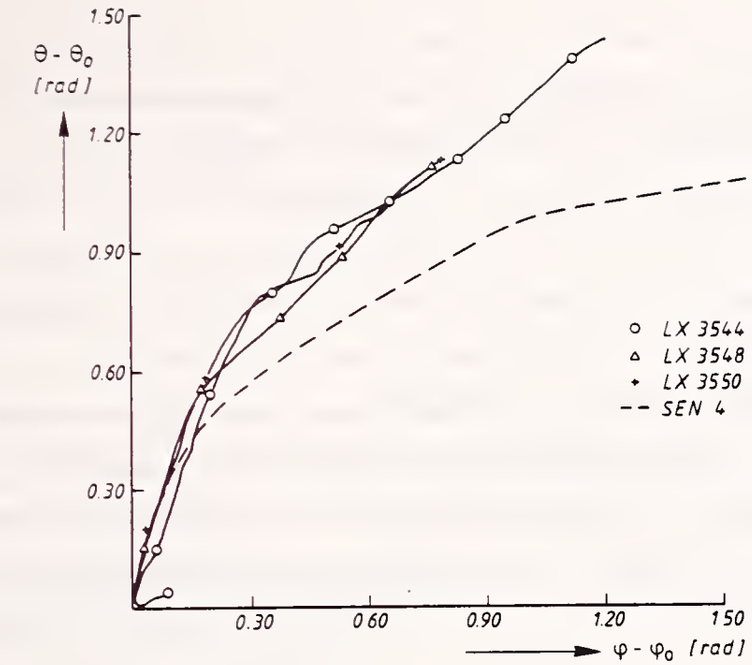

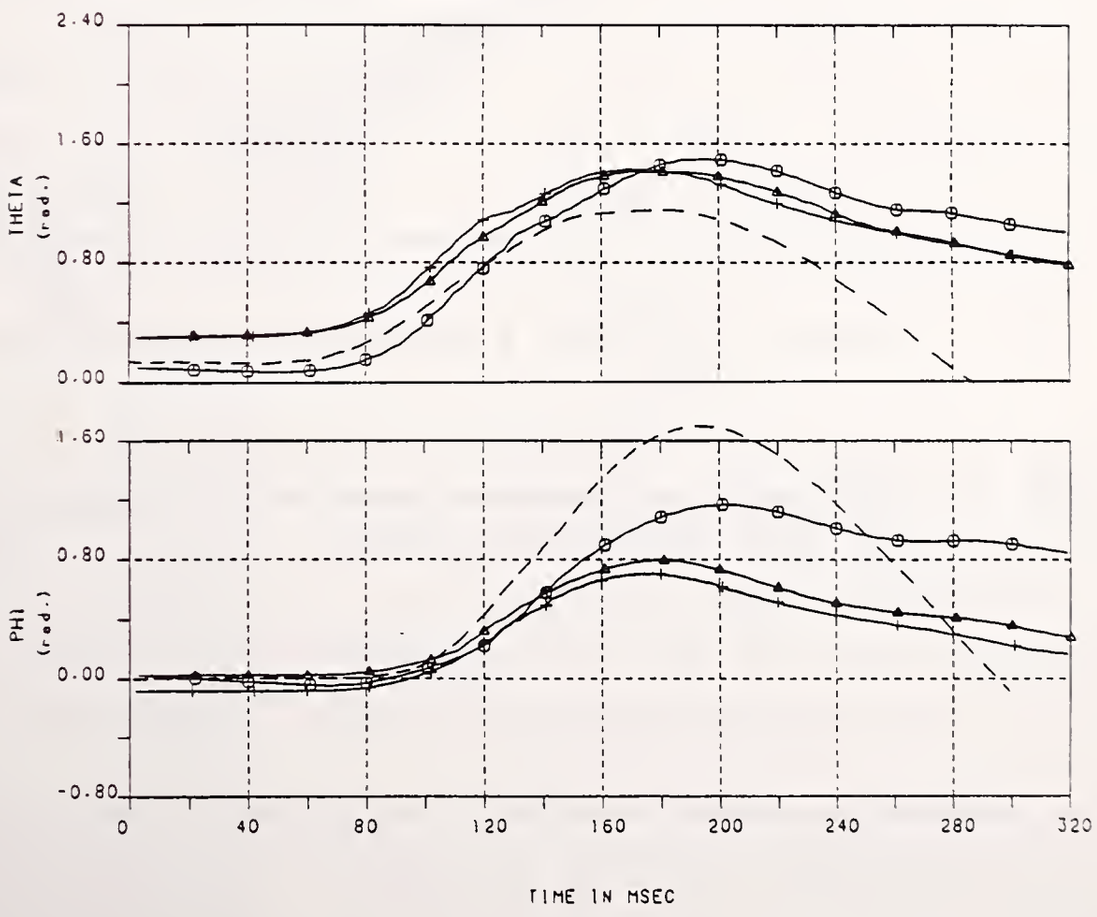

Fig. 20 Rotations for the frontal volunteer tests and a model without a locking mechanism in the upper point (SEN4).

2.6.4 The effect of the torsion stiffness of the upper pivot (oblique test)

To illustrate the influence of the torsion stiffness of the upper pivot, results of a model run with a less stiff characteristic (SEN5: 0.35 Nm/deg instead of 0.5 Nm/deg) will be presented. Fig. 21 shows that the model prediction for the head torsion ψ is improved by this change. Since the magnitude of this variation is in the same order of magnitude as the accuracy of the graphical technique used to determine this parameter, it is recommended to specify this parameter more accurately in future. Another aspect is, that the torsion stiffness has been defined from the volunteer data on the basis of a torsion angle specified as an Euler rotation about the head local z-axis. In the mathematical model a different definition is used for the torsion angle. The effect of this will be studied in a next phase of this project.

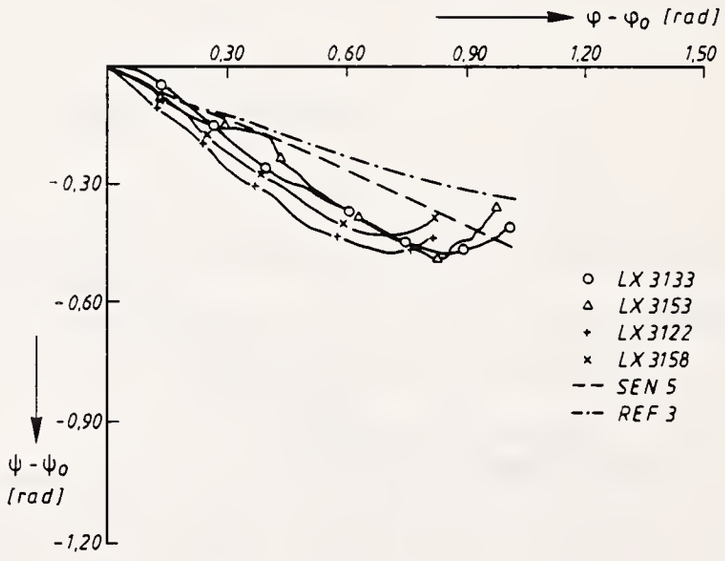

Fig. 21 Head torsion as function of head flexion resulting from model simulations and volunteer tests.

CHAPTER 3

SIMULATION OF THE PART 572 HEAD-NECK ASSEMBLY IN A STANDARD CALIBRATION TEST AND SLED TESTS

3.1 Introduction

In this chapter calibration and sled tests conducted at VRTC (2) with the Part 572 head-neck assembly will be simulated mathematically. The two-dimensional version of MADYMO will be used since only frontal test results are available. This model will be used as a design tool for Computer Aided Design (CAD) activities (see chapter 4).

The compound pendulum impact apparatus specified in FMVSS 208 Part 572 was used for the calibration tests. A detailed sketch of this set-up is shown in Fig. 22. Instrumentation includes a three-accelerometer block located at the center of gravity of the head and a fourth accelerometer mounted on the pendulum itself (see Fig. 22 for exact location). Pendulum velocity shortly before impact is measured by a light trap mounted at the accelerometer location. Head motion is measured with two rotary potentiometers, one mounted at the pendulum base and the other located at the head c.g.. The rotary potentiometers are connected by a linear potentiometer (Fig. 23).

The sled tests were conducted on a HYGE sled using a specially designed buck for mounting the head-neck assembly (Fig. 24). The impact severity for the sled test is much higher than the severity of the calibration test, 22 m/s, 35 g compared to 11 m/s, 22 g. The same instrumentation for measuring head motion and accelerations was used as in the neck pendulum calibration tests (Fig. 23). The tests are described more in detail in (2).

In the next section a description of the model set-up is presented. A more detailed description can be found in (3). Model verification will be presented in section 3.3.

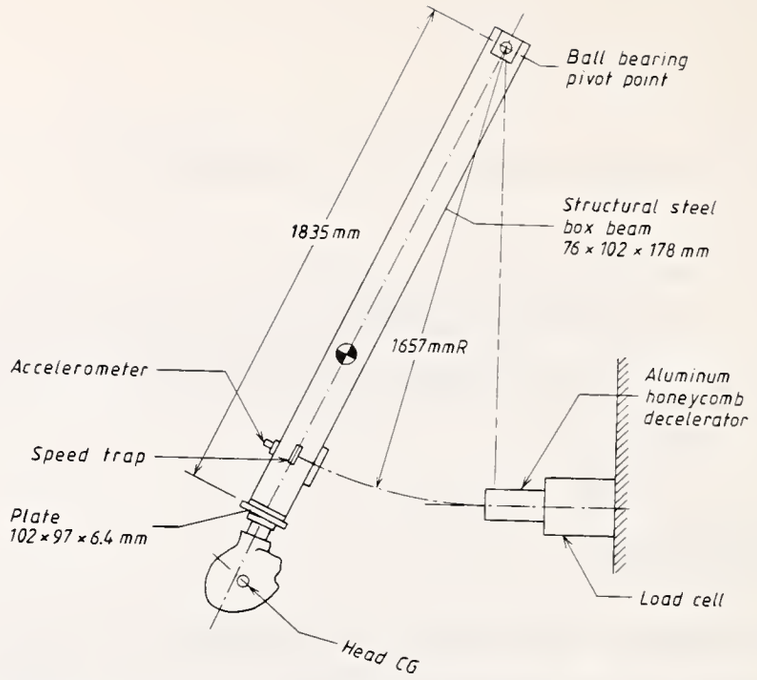

Fig. 22 Test set-up of the standard calibration test for the Part 572 head-neck assembly.

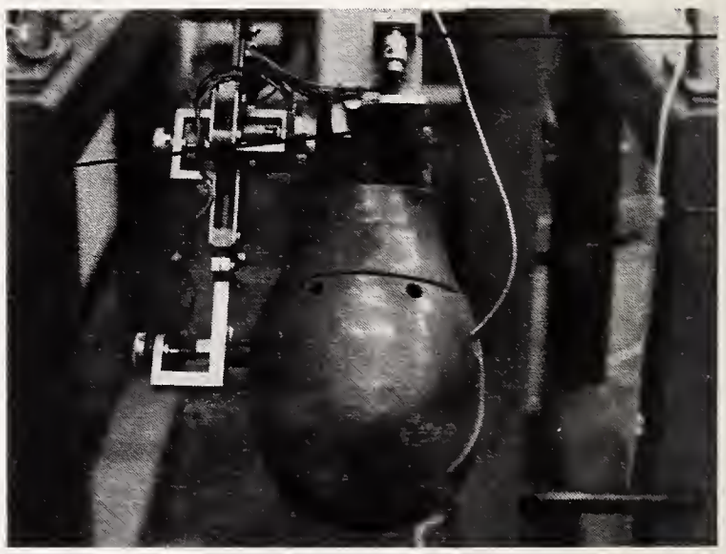

Fig. 23 Potentiometers for measuring the head-neck motions.

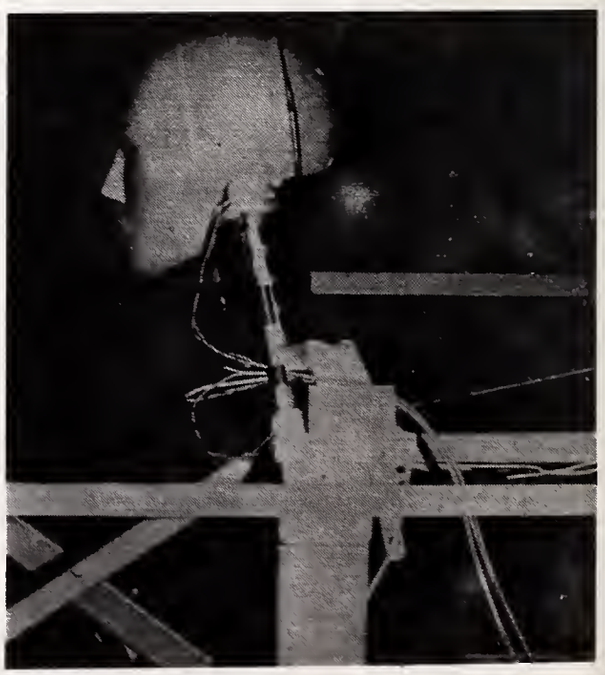

Fig. 24 Test set-up of the sled tests.

3.2 Model description

The basic set-up of the model is shown in Fig. 25. Element 1 represents the sled or pendulum. Elements 2 through 7 represent the neck, whereas the head is represented by element 8. Model input is the displacement of the neck base (element 1), i.e. the displacement (acceleration) of pendulum and the sled, respectively. The pendulum acceleration and velocity were measured at 0.20 m above the neck base (Fig. 22). Model input acceleration follows from:

$$a_i = \frac{r_a}{r_b} a_m \qquad (1)$$

where:

a_i = model input acceleration

r_a = distance between neck base and pendulum pivot (1.841 m)

r_b = distance between accelerometer and pendulum pivot (1.657 m)

a_m = measured pendulum acceleration

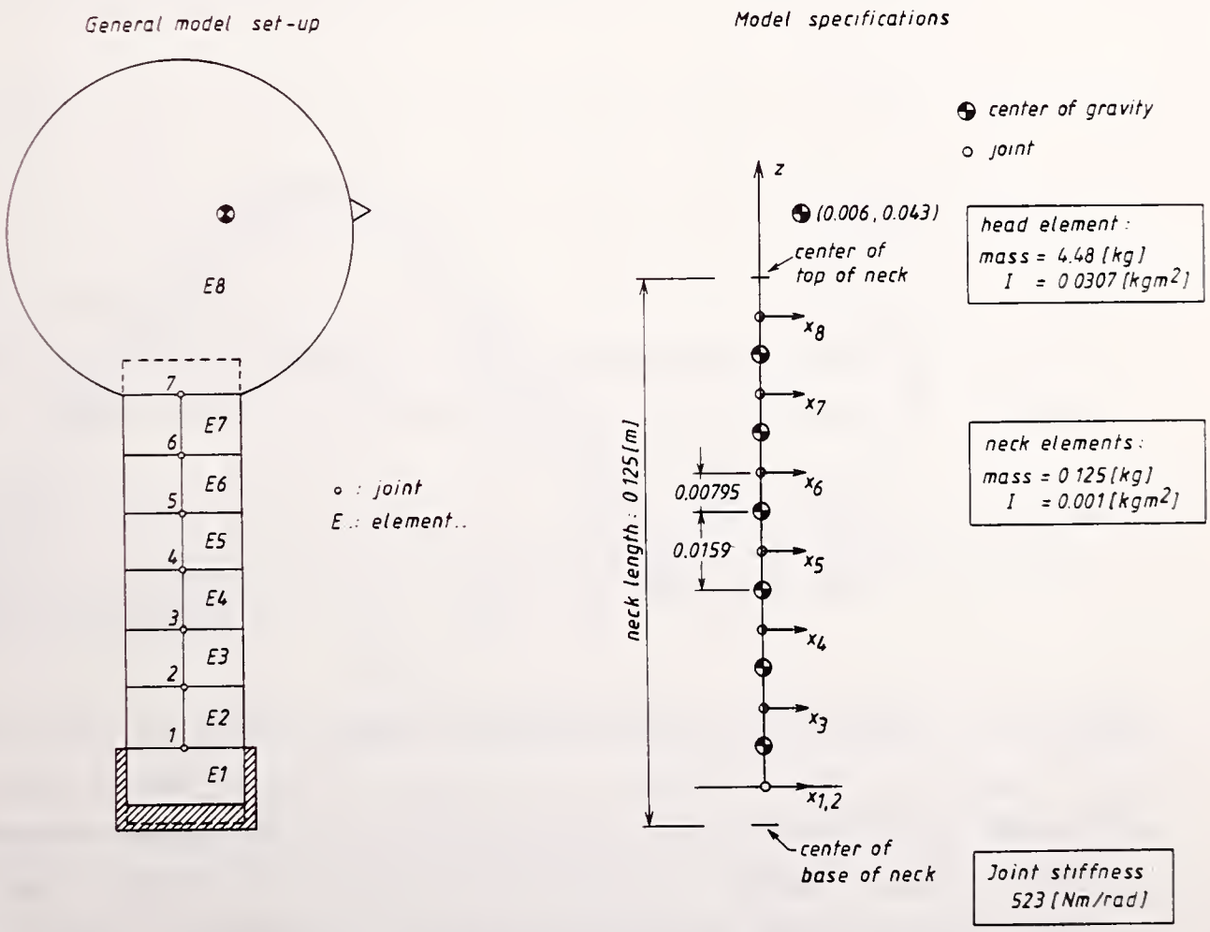

Fig. 25 General model set-up and specifications for the model of the Part 572 head-neck assembly.

The pendulum accelerations in 4 tests together with the selected model input are presented in Fig. 26. For the sled tests a simple approximation of the sled acceleration can be used as input. Fig. 27 shows an envelope of the sled accelerations in 10 similar sled tests and the corresponding model input.

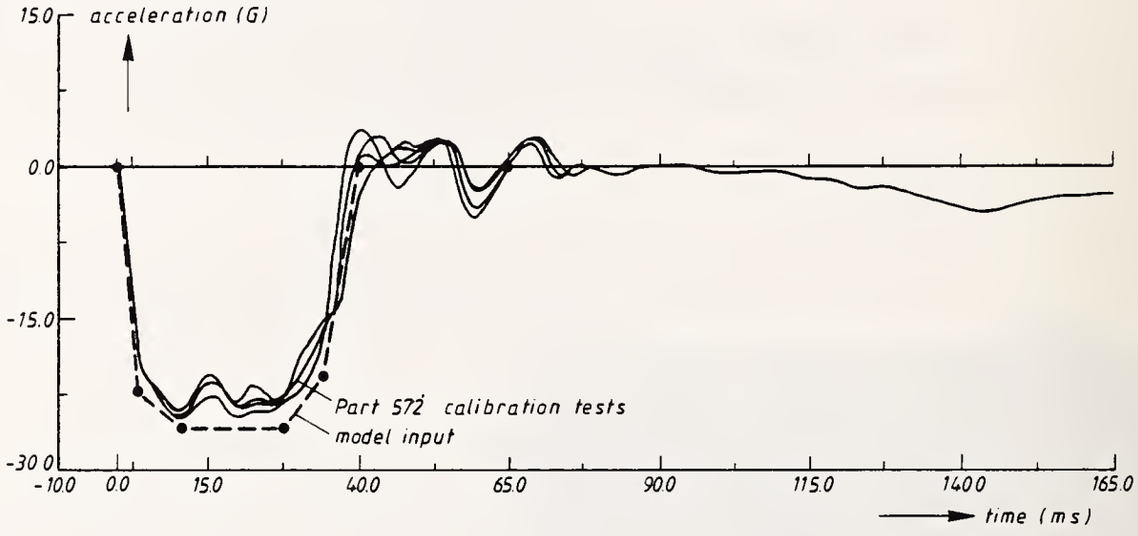

Fig. 26 Pendulum accelerations and model input.

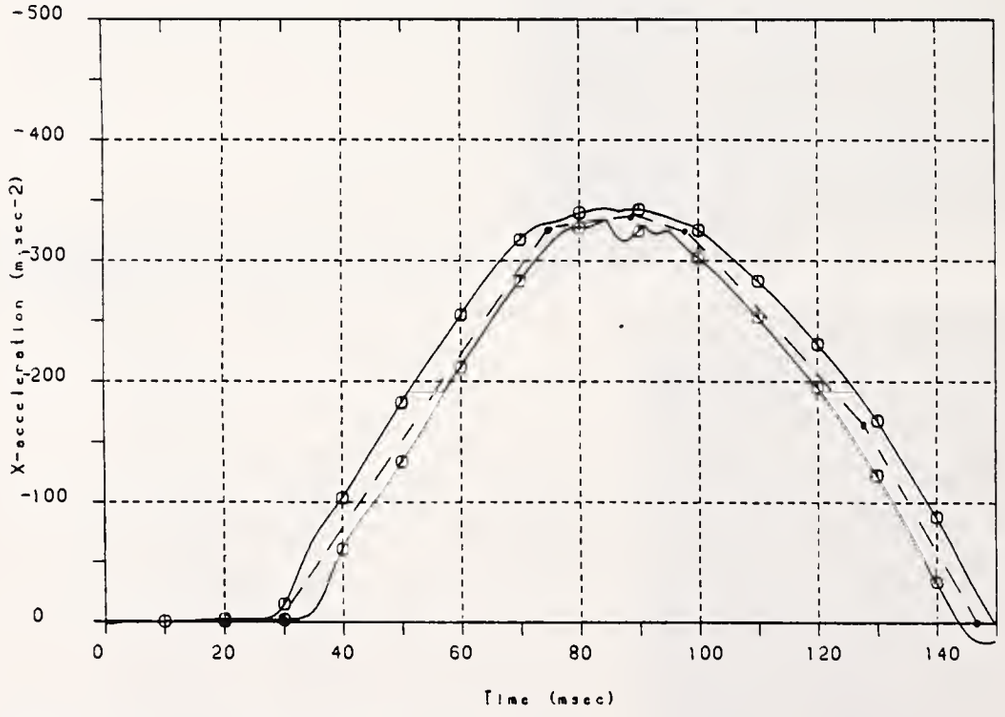

Fig. 27 Sled accelerations and model input.

The neck which is considered to be a uniform, symmetrical rubber cylinder is divided into 6 segments of equal length (Fig. 25; E2-E7). The total length of the neck is 0.111 m (excluding the steel endplates). The total neck mass is divided and assigned to the 6 rigid neck elements and partly to the head

and torso element. Mass distribution data for the head were derived from a study of the mass distribution of the complete Part 572 dummy. The results of the study are incorporated in Appendix C. The most significant model parameters are summarized in Table 3 and Fig. 25.

Table 3 Masses and moments of inertia for the 2D model of the Part 572 head-neck assembly.

	mass [kg]	moment of inertia [kg.m^2]
head element	4.48	0.0307
neck element	0.125	0.0010

MADYMO allows specification of the initial angular velocity of an element. For the Part 572 head-neck assembly in the calibration tests this angular velocity can be obtained from:

$$\omega_0 = \frac{v_0}{r_a} \qquad (2)$$

where:

ω_0 = the initial angular velocity

v_0 = the initial linear velocity at the accelerometer location (7.42 m/s)

r_a = the distance between pendulum pivot and the accelerometer (1.841 m)

The resulting angular velocity (i.e. 4.03 rad/s) is applied to the elements representing the head and neck (elements 2-8). In addition gravity is prescribed in the model.

The joint model in MADYMO 2D allows specification of elastic joint torques, viscous damping and Coulomb friction. An expression for the elastic joint torque-rotation characteristic in each joint of the model can be obtained by treating each segment of the neck as an uniform linear elastic bar loaded with moments and concentrated forces at each end (Fig. 28). If small displacements are assumed for each element the deflection equation for element i yields:

$$\Delta y_i = \frac{F_{si} \cdot (\Delta x)^3}{3EI} + \frac{M_{bi} \cdot (\Delta x)^2}{2EI} \tag{3}$$

$$\Delta \phi_i = \frac{F_{si} \cdot (\Delta x)^2}{2EI} + \frac{M_{bi} \cdot \Delta x}{EI} \tag{4}$$

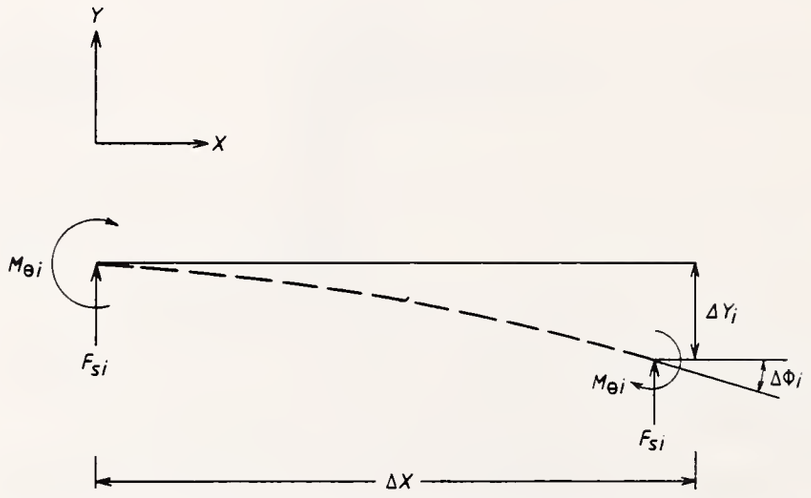

Fig. 28 Bar loaded with concentrated forces and moments.

Parameters in the above relations are explained in Fig. 28. The flexibility of this elastic segment is represented in the model by a joint located in the segment center (Fig. 29). An elastic torque function is defined for this joint as follows:

$$M = k \cdot \phi$$

Then the rotation of the joint can be described by:

$$\Delta \phi^*_i = \frac{2M_{bi} + F_{si} \cdot \Delta x}{2k_i} \tag{5}$$

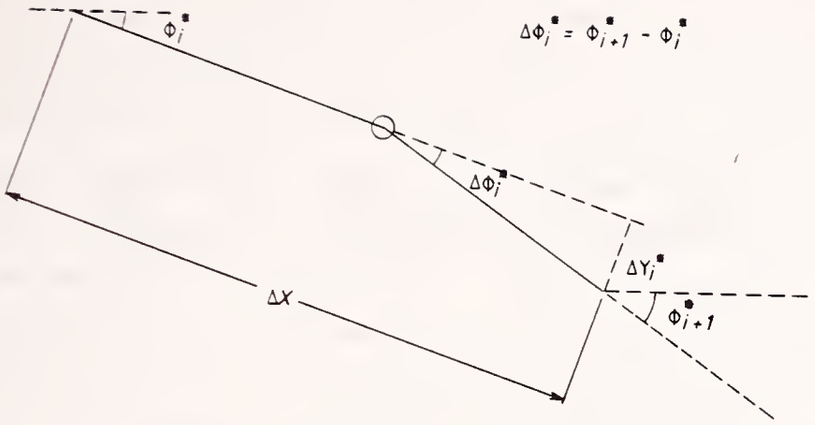

Fig. 29 Model elastic bar.

Similarly, from Fig. 29:

$$\Delta y_i^* = \frac{\Delta x}{2} \sin (\Delta\phi_i^*) \tag{6}$$

For small displacements $\sin (\Delta\phi_i^*) = \Delta\phi_i^*$ so,

$$\Delta y_i^* = \frac{2M_{bi} + F_{si} \cdot \Delta x}{2k_i} \cdot \frac{\Delta x}{2} \tag{7}$$

To determine a value of k_i which makes the linkage behave like an elastic bar, equate the expressions obtained for rotations ((4) and (5)). This yields:

$$\Delta\phi_i = \Delta\phi_i^*$$

$$\frac{F_{si} \cdot (\Delta x)^2}{2EI} + \frac{M_{bi} \cdot \Delta x}{EI} = \frac{2M_{bi} + F_{si} \cdot \Delta x}{2k_i}$$

This reduces to:

$$k_i = \frac{EI}{\Delta x} \tag{8}$$

Alternately, equate the expressions for displacements ((3)) and (7)). This yields:

$$\Delta Y_i = \Delta Y_i^*$$

$$\frac{F_{si} \cdot (\Delta x)^3}{3EI} + \frac{M_{bi} \cdot (\Delta x)^2}{2EI} = \frac{F_{si} \cdot (\Delta x)^2}{4k_i} + \frac{M_{bi} \cdot (\Delta x)}{2k_i}$$

or:

$$k_i = \frac{EI}{\Delta x} \cdot \frac{3F_{si} \cdot \Delta x + 6M_{bi}}{4F_{si} \cdot \Delta x + 6M_{bi}} \qquad (9)$$

If Δx is quite small this relation reduces to:

$$k_i = \frac{EI}{\Delta x}$$

This is identical to the expression obtained from consideration of rotations. An average value of EI=8.32 [Nm^2] was determined from published static bending test data (4,5). The corresponding elastic joint stiffness is 523 [Nm/rad]. The damping coefficient required for critical damping in each joint was estimated by analyzing a one-degree-of freedom system. This analysis resulted in a critical damping coefficient for flexion of 1.45 [Nms/rad].

3.3 Model validation

In order to validate this model, corridors have been determined using results from the sled tests and the calibration tests. The following parameters will be used for validation:

- the head rotation,
- the horizontal (x) and vertical (z) displacements of the head c.g. relative to the neck base,
- the horizontal (x) and vertical (z) accelerations of the head c.g.

Three different simulations have been conducted for the calibration tests, namely with undamped, "50% critically" (0.75 [Nms/rad]) and "critically" damped (1.45 [Nms/rad]) neck joints. Results from these simulations are shown in Fig. 30. Reliable model results are obtained for the head rotations, the vertical head displacement and the linear accelerations. Relatively large deviations can be observed, however, for the horizontal displacements, which can be explained by the absence of shear and elongation in the model. From the model results it appears that the "50% critically" damped model provides the most realistic results. So this model will be used for further validation at a higher impact severity level (sled test). Fig. 31 shows the results of this simulation together with the experimental corridors. Here, too, quite realistic results are obtained from the simulations, except, for the horizontal displacements, as could be expected.

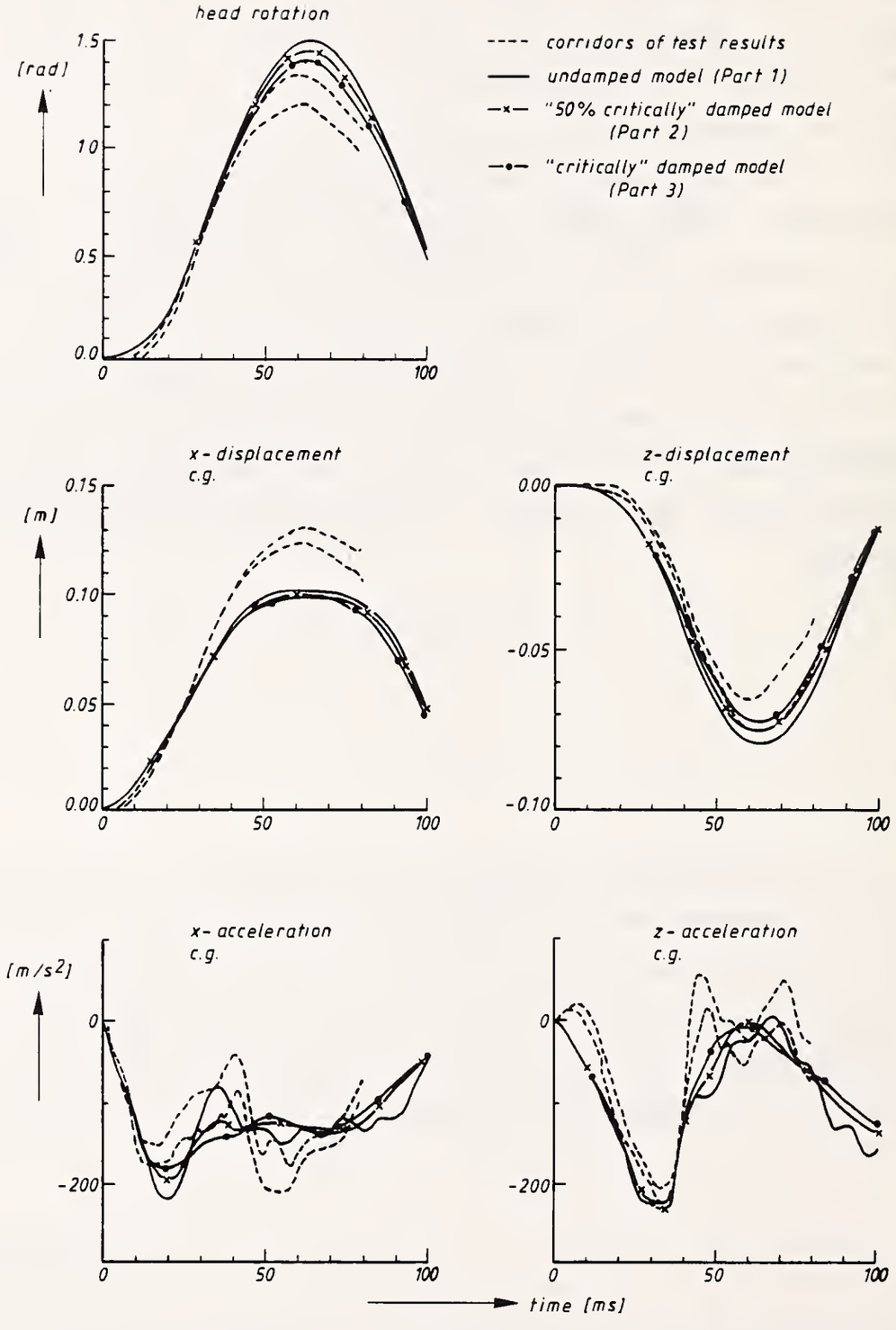

Fig. 30 Model and test results of the standard calibration tests.

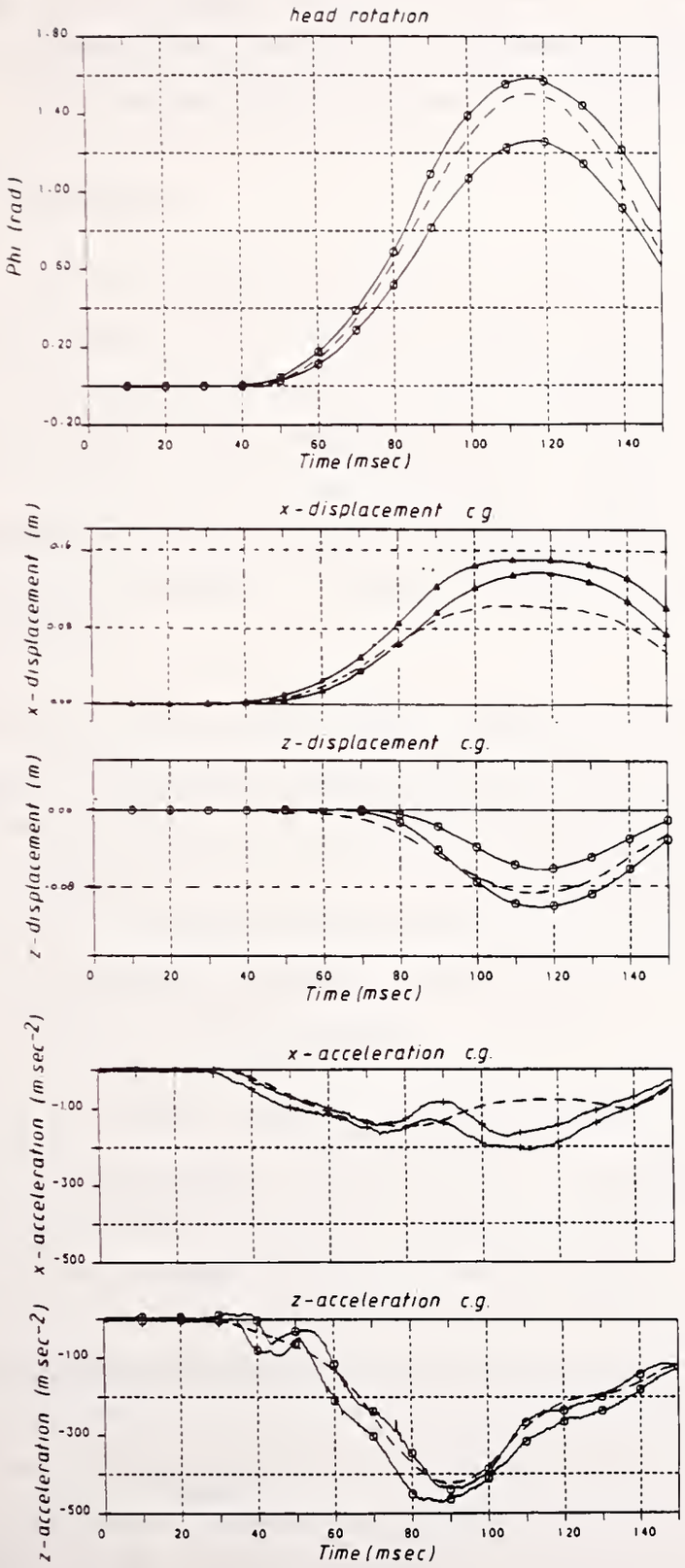

Fig. 31 Model and test results of the sled tests.

Based on these simulations it can be concluded that this model offers a realistic simulation for the behaviour of the Part 572 dummy head-neck assembly in frontal impacts. Although the model significantly underestimates the horizontal head displacement, this is not considered to be a major drawback for use of the model as a computer aided design tool.

CHAPTER 4

COMPUTER AIDED DESIGN OF AN IMPROVED MECHANICAL HEAD-NECK ASSEMBLY

4.1 Introduction

The Part 572 (Hybrid II) neck was designed to perform realistically in frontal impacts. In a study by Muzzy and Lustick (6) displacements of the Hybrid II head-neck system were compared with human volunteers in 10 g frontal impacts. The complete dummy was tested in a restraint system similar to that of the human volunteers. Significant differences in the displacements of the head center of gravity and the head angle relative to the torso were observed: the Hybrid II neck was found to be stiffer than the volunteer's.

In section 4.2 a more direct comparison between the Part 572 head-neck assembly and human volunteer behaviour will be presented by prescribing the measured human volunteer T1 acceleration directly to the base of the neck. In this way test data are not diffused, for instance by the thorax compliance. The more recent Hybrid III head-neck system which, like the Part 572 head-neck assembly, was designed for frontal biofidelity is also incorporated in this experimental evaluation.

Section 4.3 deals with preliminary computer aided design activities conducted in this study. Results will be presented of design changes introduced in the Part 572 neck in order to improve the mechanical behaviour in view of the findings from the volunteer tests.

4.2 Comparison between existing neck designs and volunteer necks

The Part 572 and Hybrid III neck were both designed to perform realistically in frontal impacts. At the Vehicle Research and Test Center an experimental study has been conducted as part of the "New Car Assessment Test Procedure Analysis" project, in which both necks were exposed to various impact levels (2). In one of the tests the sled acceleration pulse was based on the most severe NBDL human volunteer test, i.e. subject H00093 in

test LX3616. Both dummy head-neck assemblies were equipped with one translational and two rotary potentiometers in order to determine the relative head displacements.

Fig. 32 presents occipital condyle trajectories calculated from the instrumentation data together with the human volunteer trajectory of test LX3616.

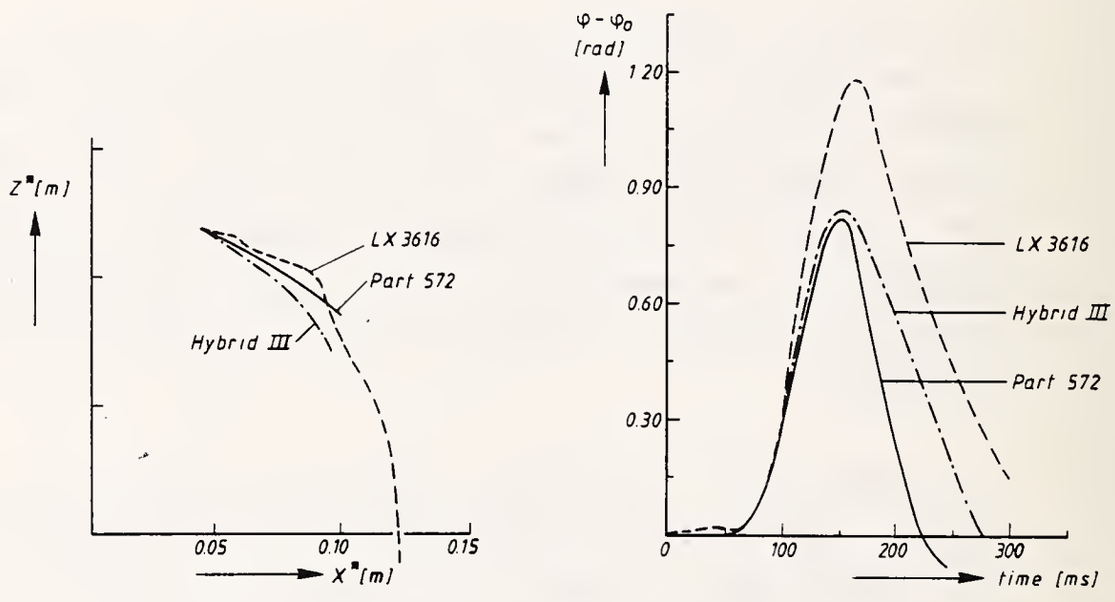

Fig. 32 Occipital condyle trajectories and head rotation in two dummy neck designs and the most severe human volunteer test.

For the dummy head-neck assemblies the occipital condyles are assumed to coincide with the center of the head-neck connection. Head rotation-time histories for dummies and volunteer are also shown in this figure. It follows that head rotation and horizontal o.c. displacements are slightly smaller for both head-neck assemblies than they are for volunteers. Much larger deviations, however, can be observed for the vertical displacements: both neck designs appear to be stiff in comparison with the volunteer behaviour*. These differences between dummy and volunteer are even more apparent if one considers that subject H00093 shows relatively small head excursions compared to subject H00083.

---

* In ref. (7) and ref. (8) center of gravity trajectories for dummy and volunteer were compared rather than the occipital condyle trajectories. Due to an error in the data processing, however, volunteer c.g. trajectories and peak c.g. displacements were not presented completely correct in these references. The effect of this in view of the large deviations between dummy and volunteer behaviour is small.

4.3 Design variations

By means of the mathematical Part 572 head-neck model (PART2) presented in the preceding chapter, the effect of various changes in the Part 572 neck design will be evaluated. Results of 4 interesting design principles will be presented here:

CAD1: reduced neck stiffness (50%)

CAD2: reduced neck stiffness (50%) and a free range of motion with locking mechanism in the head-neck connection

CAD3: longer neck with a reduced neck stiffness (50%) where the neck is connected to the head 4 cm above the center of gravity

CAD4: very soft neck (stiffness about 10% of original Part 572 neck stiffness) reinforced at the front and back by two relatively stiff springs.

Fig. 33 illustrates these design principles together with the reference model. In order to introduce the locking mechanism in the second variation, the existing joint model in MADYMO 2D was modified in accordance with the simulation of the locking mechanism in the 2-pivot model presented in section 2.3.

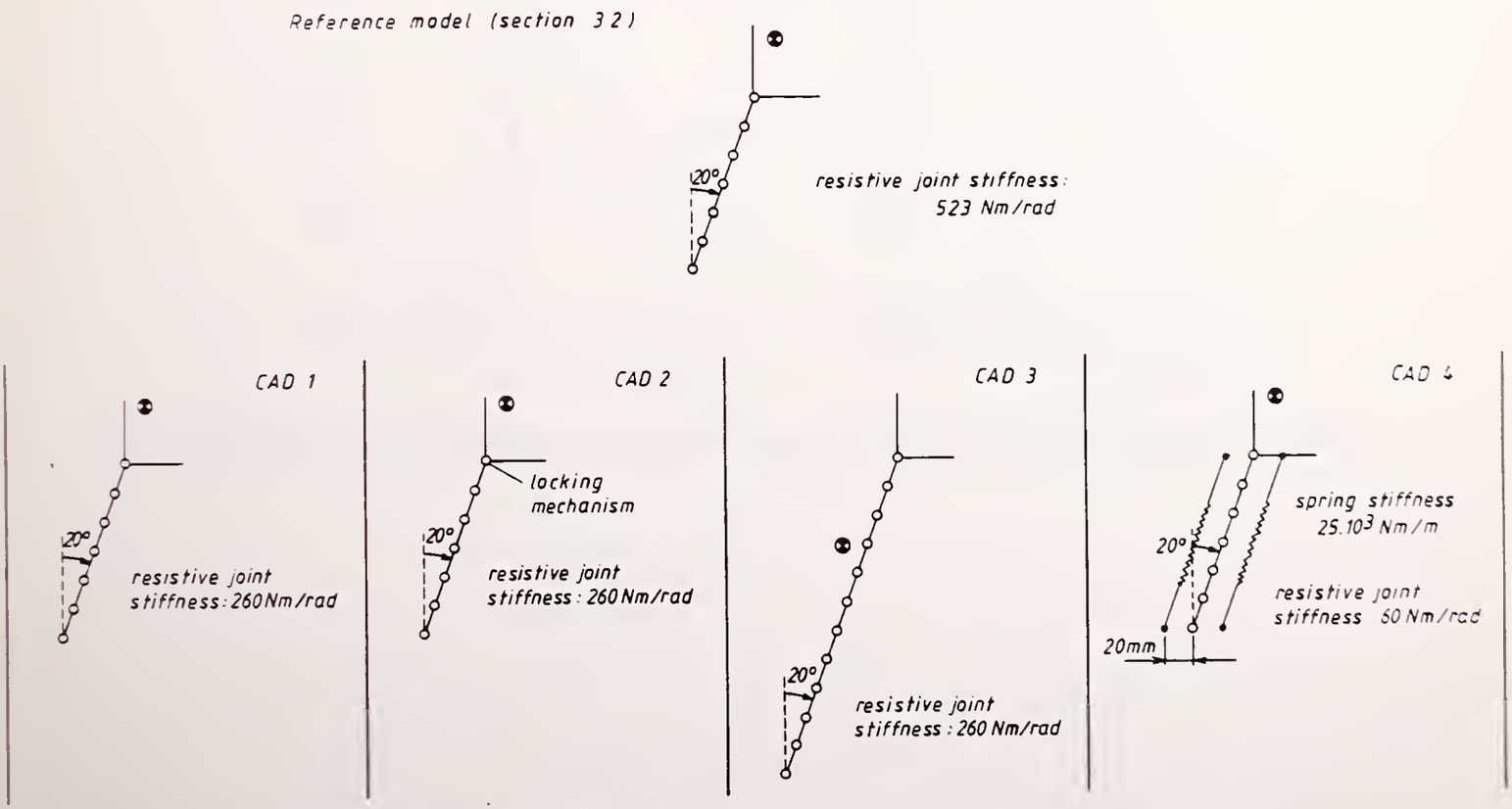

Fig. 33 Design changes in the standard Part 572 head-neck assembly.

For each design change two simulations are conducted, i.e. a simulation of the most severe frontal volunteer test (test LX3616) and a simulation of a set of moderate tests (tests LX3544, LX3548 and LX3550). Approximations for the T1 accelerations of the volunteer tests will be used as model input (Figs. 8 and 15).

4.4 Model results

Results of the model simulations together with human volunteer test results are presented in Figs. 34-37. The upper sections of these figures show the occipital condyle trajectories. For the human volunteer tests these trajectories are presented relative to the corrected T1 coordinate system. For the model simulations these results represent the trajectories of the center of the neck top relative to a coordinate system with its origin in the center of the neck base and with the same orientation as the laboratory coordinate system. The lower section shows results for the head rotations as function of time.

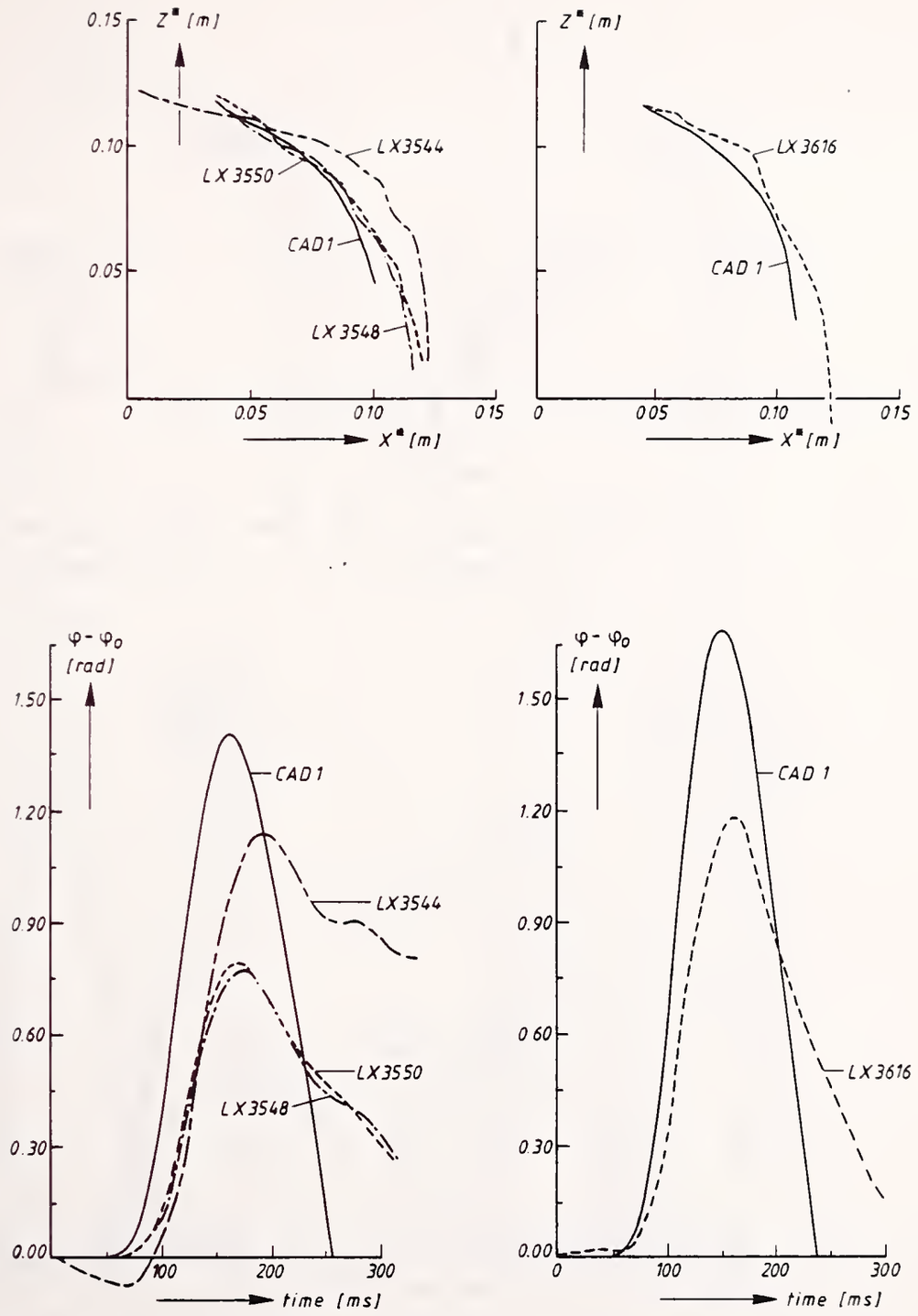

Fig. 34 Occipital condyle trajectories and rotation-time histories (CAD1).

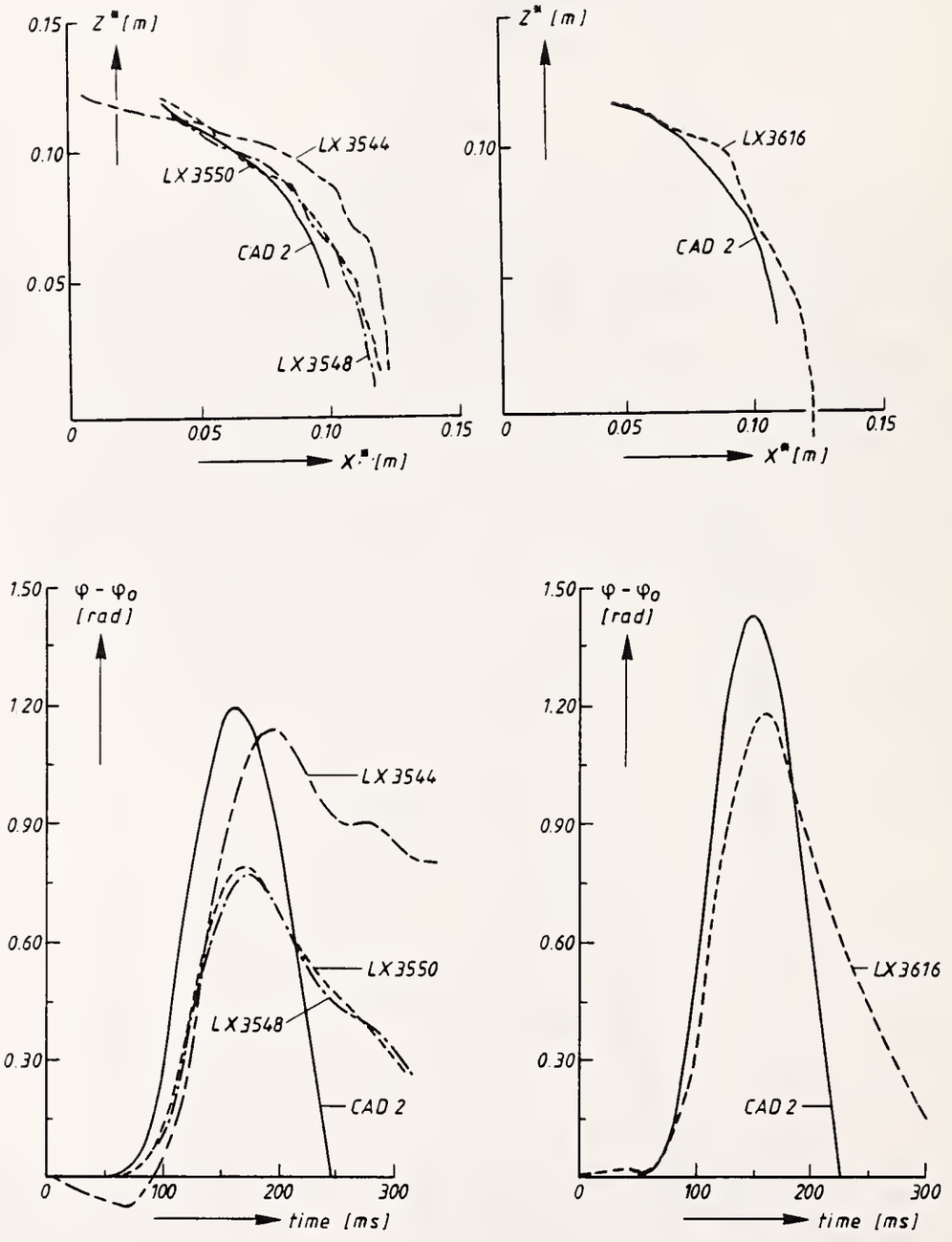

Fig. 35 Occipital condyle trajectories and rotation-time histories (CAD2).

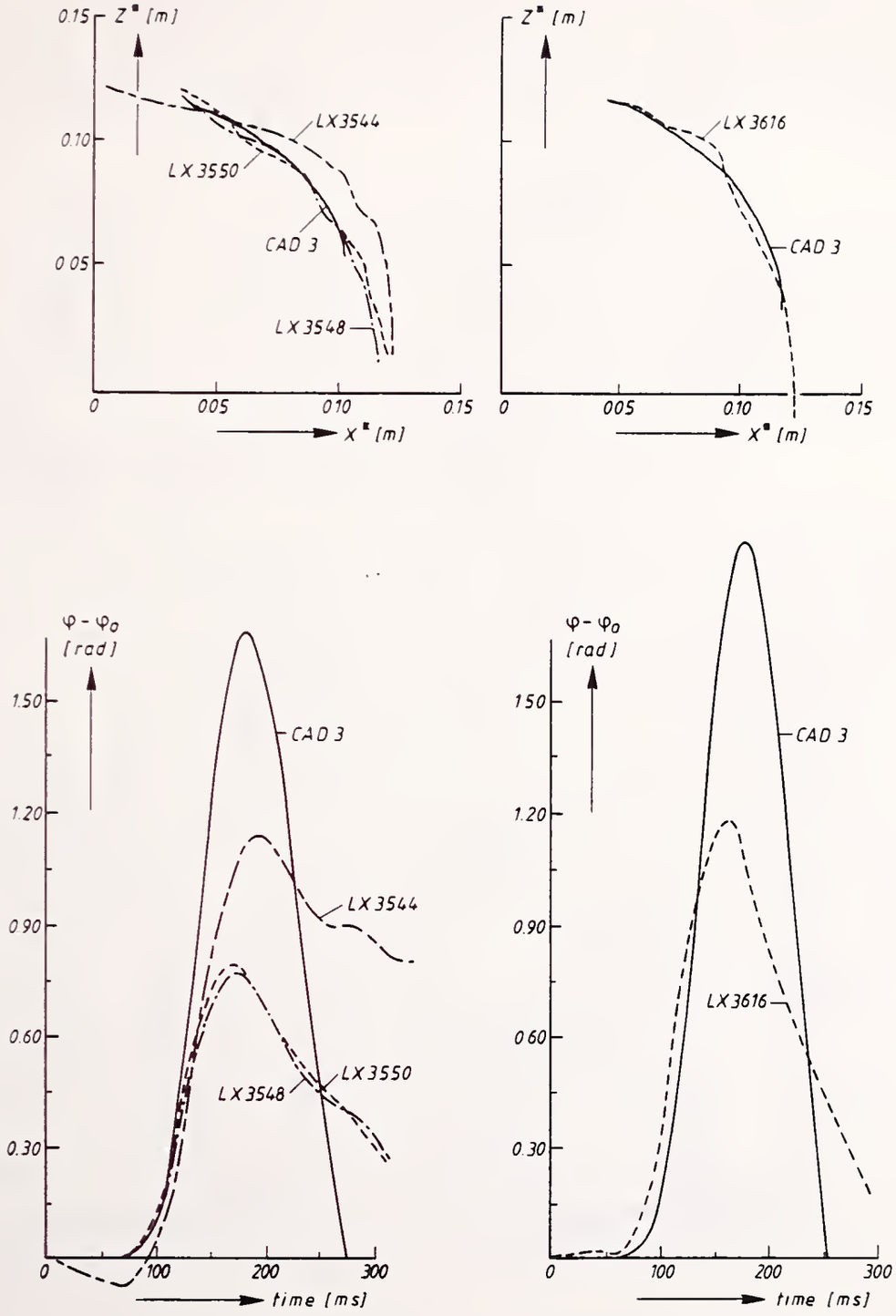

Fig. 36 Occipital condyle trajectories and rotation-time histories (CAD3).

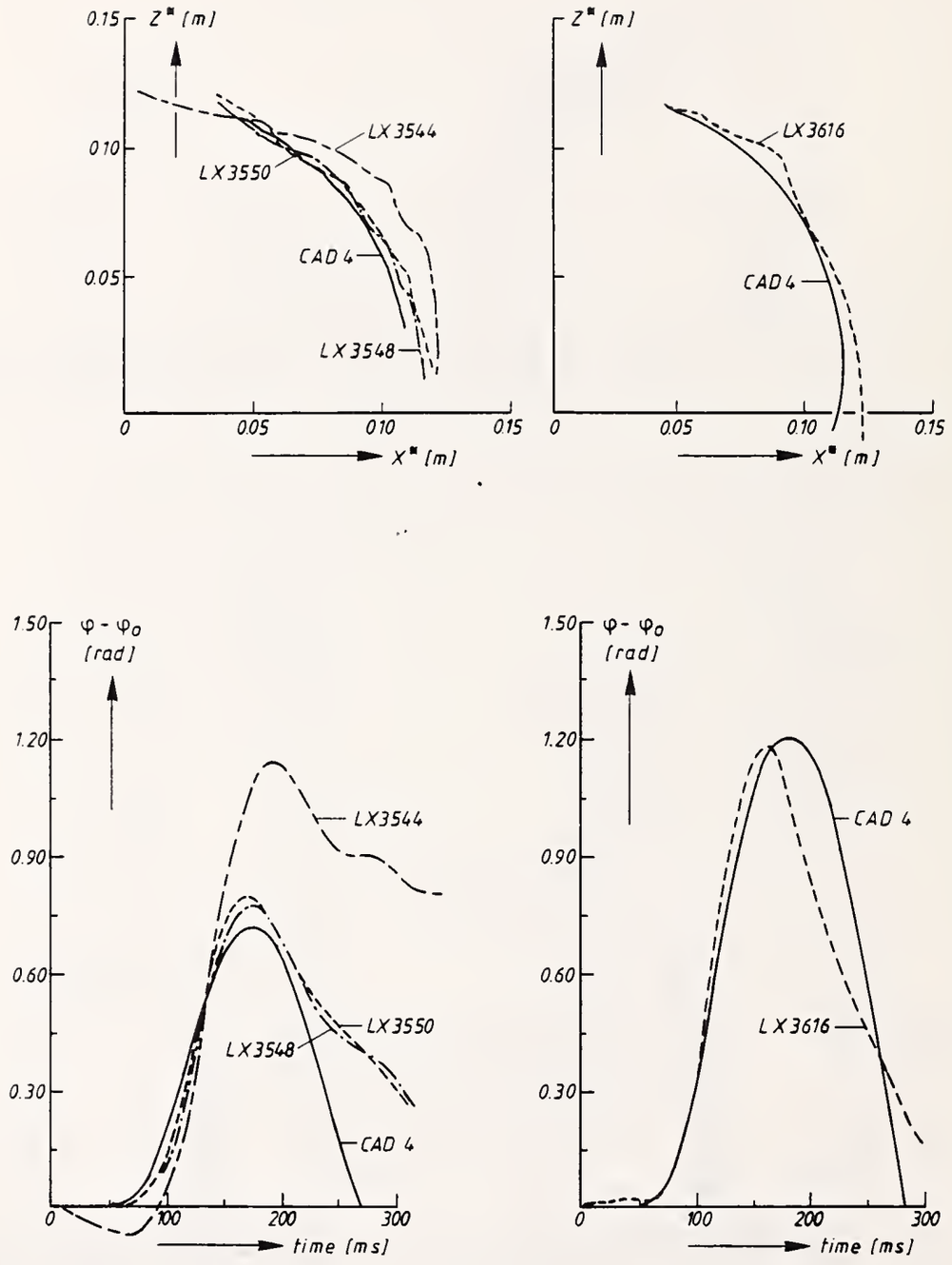

Fig. 37 Occipital condyle trajectories and rotation-time histories (CAD4).

Fig. 34 shows the results for a halved neck stiffness (CAD1). Although a much better approximation of the occipital condyle trajectories is obtained by this design change, still the head excursion appears to be too small. On the other hand head rotations are much larger now than in the human volunteer tests.

By means of simulation CAD2 an attempt is made to reduce the head rotation by introduction of a free range of motion with a locking mechanism in the top of the neck as could be observed in the human volunteer tests. With this design change the o.c. trajectory is not affected while the head rotation is indeed slightly reduced compared to CAD1 (Fig. 35).

In the preceding design modifications the geometrical configuration of the neck was not changed. Simulation CAD3 considers the effect of a much longer neck (almost twice as long) which is connected in the head above the center of gravity. In addition the neck stiffness is halved as in the variations CAD1 and CAD2. This design change results in o.c. trajectories similar to those resulting from CAD1 and CAD2 (the o.c. location relative to the head reference frame is identical to CAD1 and CAD2). The head rotation as function of time appears to be improved in the initial phase of the motion (up to 125 ms) compared to CAD1 and CAD2. For larger time values, however, the rotation strongly increases resulting in a much larger peak head rotation. Fig. 38 roughly illustrates this behaviour. Up to 125-150 ms the head c.g. is located below the connection of the head to the neck resulting in a negative torque applied to the head due to the impact acceleration forces. Consequently positive rotation of the head will be limited. For larger time values, however, the head c.g. passes the head-neck connection and the impact acceleration field which is still active will now cause a positive torque on the head.

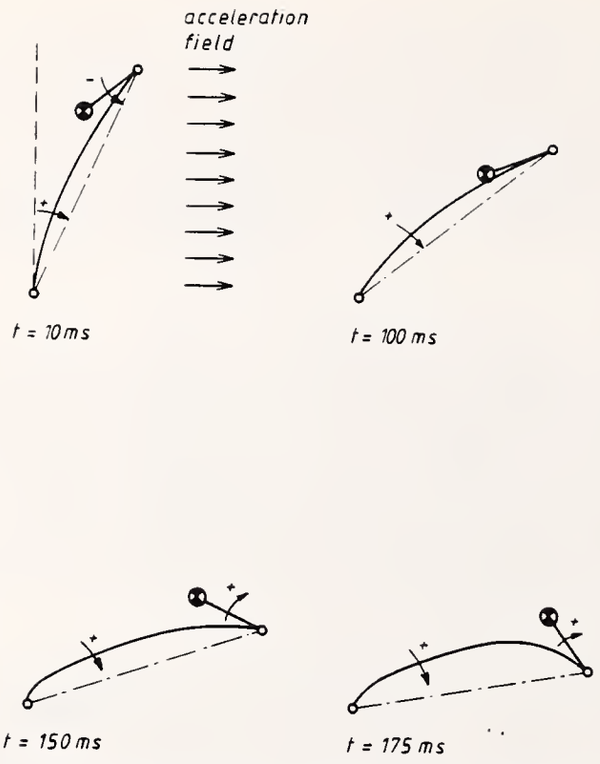

Fig. 38 Kinematics for simulation CAD3.

Results of the final design change to be considered here (i.e. CAD4) are presented in Fig. 36. The geometrical properties of this design are identical to the Part 572 neck. The neck stiffness is reduced by a factor of almost 10. At a distance of 2 cm from the neck centerline two relatively stiff springs are located between the torso and the head, one spring at the front side and one at the back side. In this way the head-neck system is expected to behave more or less like a four bar linkage mechanism where the torso, head and the individual springs represent one bar. Results of this simulation appear to be very realistic (Fig. 37). Resulting linear and angular accelerations are presented together with volunteer test results in Fig. 39. These results appear to be quite realistic.

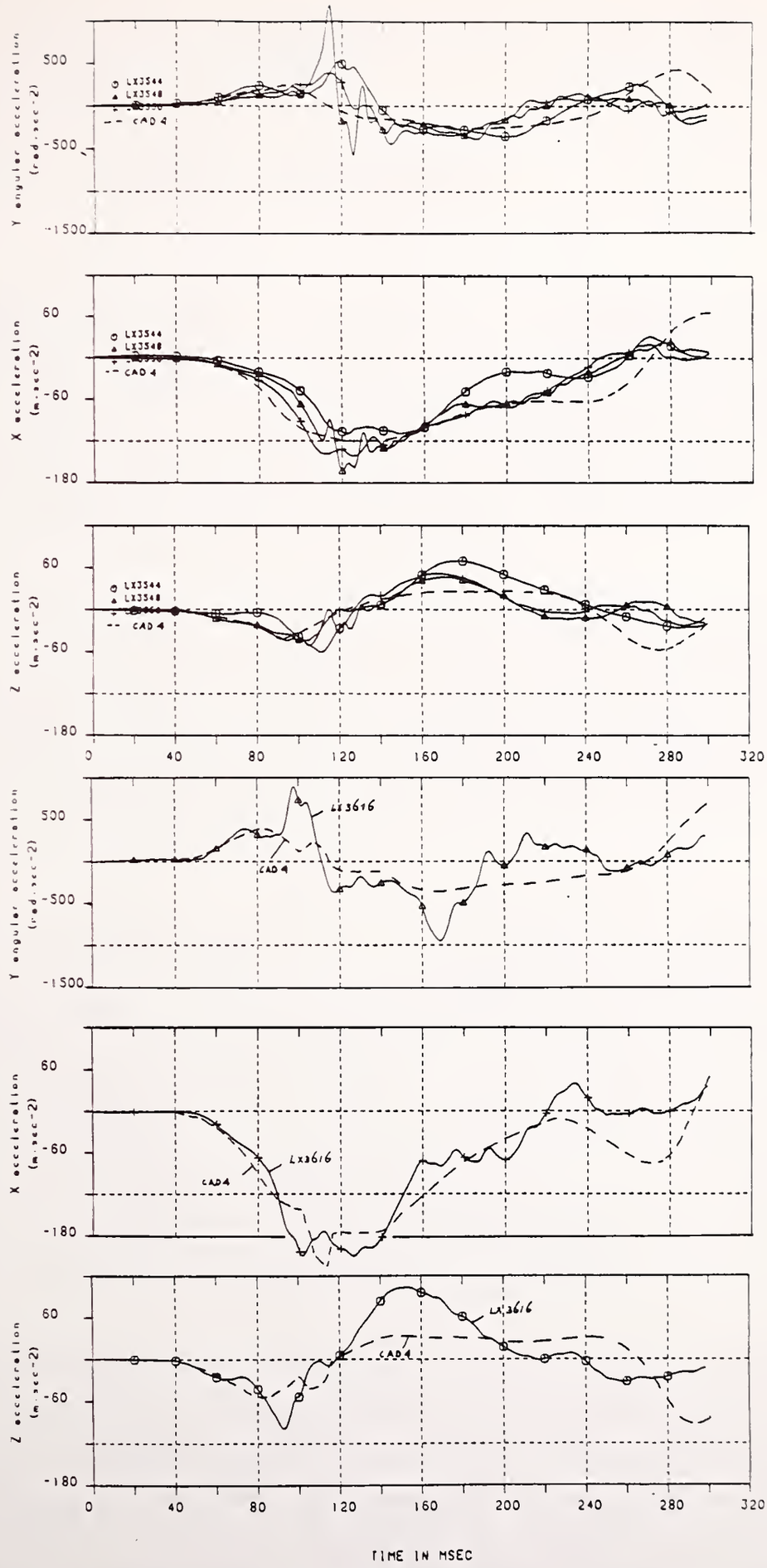

Fig. 39 Comparison of accelerations of the anatomical origin in laboratory directions in moderate frontal volunteer tests and in the most severe frontal volunteer test and simulation CAD4.

CHAPTER 5

DISCUSSION AND CONCLUSIONS

The study presented here summarizes a number of mathematical simulation activities conducted in phase I of the VRTC head-neck research program. The activities can be subdivided into three categories, namely, the validation of the analog system concept proposed in Vol. I of this final report, the formulation of a mathematical model for the Part 572 dummy head-neck assembly and some preliminary computer aided design activities.

The model simulations presented in chapter 2 for verification of the analog systems show that the proposed 2-pivot linkage mechanisms provide a realistic representation of the human volunteer behaviour. Model results appear to be close to the human volunteer test results with two exceptions: the relative rotation in the upper pivot in frontal impacts and the head torsion in oblique impacts are found to be too small.

The sensitivity study presented in section 2.6 reveals that an improvement in the simulations with respect to the above deficiencies might be expected if the lower pivot torque data (i.e. in the torso center of rotation) are determined directly from the human volunteer data rather than estimated from T1 origin torque calculations. Instead of linear approximations for the pivot stiffness characteristics the use of piece-wise linear or higher order functions should be considered. The limited accuracy of the graphical techniques used to approximate the human volunteer torque-rotation characteristics could be improved by using numerical techniques.

The underestimation by the model of the head torsion in case of oblique impacts might also be caused by the different ways in which the torsion angle is defined in the volunteer tests and the model. In the volunteer tests torsion is defined by third Euler angle, while in the model as a consequnce of the introduction of the flexion-torsion model, torsion is defined in a slightly different way (see section 2.3). The influence of this is not completely clear yet and is subject of further research. The system parameters

for the analog systems relate to average estimations from tests with two different subjects. A calculation showed that model predictions can be improved slightly by the introduction of subject specific data rather than average data.

The second model activity in this study deals with a model of the Part 572 dummy head-neck assembly. The neck section in this model is represented by 6 rigid segments connected by pin joints. Model verification was conducted for two different impact severities: the standard neck calibration test and a more severe sled test. Realistic model predictions were obtained, except for the horizontal head displacements. Differences in displacements can be explained by the absence of elongation and shear in this model. This deficiency is not considered to be a serious limitation for use of the model as a computer aided design tool. If necessary model predictions can be roughly corrected for the underestimation of this output parameter. If such a correction is introduced in the simulation results of the design examples in chapter 4, model predictions in general would improve with respect to the volunteer behaviour. In future simulations, representation of the Part 572 neck could be improved by the development of a special flexible element in MADYMO.

Experimental evaluation of the Part 572 and Hybrid III neck system with respect to the volunteer behaviour showed that both necks are too stiff, particularly for the vertical displacement of the head (chapter 4). Mathematical simulations have been conducted (see chapter 4) in order to optimize the design of the Part 572 neck in view of the findings from the volunteer tests. The first results of these computer aided design efforts are quite promising. The best results up to now are obtained from a design that consists of a soft neck reinforced by a relatively stiff structure in the front and the back section. The overall size of this neck is the same as in the present Part 572 neck. A possible realization of such a design principle is a soft rubber cylinder imbedded by strong fibres or provided with one or more separate stiff rubber segments. Building one or more prototypes according to this design principle and experimentally evaluating them under test conditions representative of the most severe human volunteer test (i.e. run LX3616, 15 g, 17 m/s) is strongly recommended.

The primary aim of the computer aided design activities described here was the evaluation of the feasilibity of the model as a computer aided design tool. Results presented here relate to only a limited set of possible design principles. A more systematic approach could lead to other attractive design concepts. Such an analysis should not be limited to the neck design itself but should also address the neck location relative to thorax and head, the head mass distribution and the head-chest interaction. In the present analysis, for instance, human volunteer occipital condyles are assumed to coincide with the center of the neck top. In this way, however, volunteer head center of gravity and dummy head center of gravity will not be in the same position (deviation 0.032 m).

Results presented here are valid only for relatively low g-levels. One subject in the present database was exposed to the most severe impact condition i.e. 17 m/s and 15 g. New volunteer test results which recently have been obtained from NBDL, include several tests for this impact severity level. In addition cadaver test results should be obtained for higher impact levels. The locking mechanism observed in the volunteer tests will most likely be absent in cadaver tests. A simulation which was conducted in section 2.6.3 showed a larger head rotation in this situation and the so-called tipping over of the head link relative to the neck link.

It is expected that computer aided design activities in close interaction with the development and testing of promising neck prototypes will lead to a neck with frontal biofidelity. Once such a neck is obtained the analysis can be extended to a neck with omni-directional biofidelity.

ACKNOWLEDGMENTS

This study has been supported by the Department of Transportation/National Highway Traffic Safety Administration. All opinions given in this report are those of the authors, and not necessarily those of DOT/NHTSA.

The authors wish to express their gratitude to the staff of the Naval Biodynamics Laboratory in New Orleans for providing the human volunteer test data and the additional information necessary to perform this analysis; to J. Hofferberth and T. Hoyt of the Vehicle Research and Test Center, East Liberty (Ohio) and R. Eppinger and R. Morgan of the Office of Vehicle Research, Washington D.C., for their guidance and valuable suggestions; to R. Stalnaker and D. Guenther of the Ohio State University, Columbus (Ohio) for their general support; to M. Cline of the Transportation Research Center, East Liberty (Ohio), D. Gordon of Systems Development Corporation in Cambridge and M. de Bruin and L. Wittebrood of the Research Institute of Road Vehicles TNO, Delft, The Netherlands for the processing of the test results; to C. Spenny of the Transportation Research Center in Cambridge who was responsible for the neck load calculations; to R. Saul of the Vehicle Research and Test Center, East Liberty (Ohio), who provided the dummy-neck test data; to M. Farris and J. Lyn of the Ohio State University Columbus (Ohio), for their contribution in the MADYMO simulations.

REFERENCES

1. Wismans, J., Hoen, T. and Wittebrood, L. (1985):
Status of the MADYMO Crash Victim Simulation Package 1985. Presented at 10th International Conference on "Experimental Safety Vehicles", Oxford, England.

2. "New Car Assessment Test Procedure Analysis". Draft Report Phase II, Project SRL-82, Neck repeatability testing (not yet published), Vehicle Research and Test Center - East Liberty, Ohio, USA.

3. Farris, M.V. (1983):
"A Mathematical Model Simulating the Dynamic Response of the Part 572 Anthropomorphic Crash Test Dummy Neck". A thesis presented in Partial Fulfilment of the Requirements for the Degree Master of Science. Ohio State University.

4. Fleck, J.T., Butler, F.E. and Deleys, J.J. (1982)
"Validation of the Crash Victim Simulator". Engineering Manual, vol. 2, Part II: Validation Effort, Department of Transportation Report No. ZS-5881-V-2, Calspan Corporation, Buffalo, NY, USA.

5. Hasselman, J. and Wismans, J.S.H.M. (1980):
"Drie-dimensionale dummiekarakteristieken t.b.v. MADYMO - Computersimulaties", Report No. 700120002-H, Research Institute for Road Vehicles, Delft, Netherlands.

6. Muzzy III, W.H. and Lustick, L. (1976):
"Comparison of Kinematic Parameters Between Hybrid II Head and Neck System with Human Volunteers for - Gx Acceleration Profiles". In: Proceedings of the 20th Stapp Car Crash Conference, SAE Paper No. 760801.

7. Wismans, J. and Spenny, C.H. (1983):
"Performance requirements for mechanical necks in lateral flexion". In: Proceedings of the 27th Stapp Car Crash Conference, SAE, Paper No. 831613.

8. Wismans, J. and Spenny, C.H. (1984):
"Head-neck response in frontal flexion". In: Proceedings of the 28th Stapp Car Crash Conference.

APPENDIX A

FLEXION - TORSION MODEL

A1 INTRODUCTION

For the simulations presented in chapter 2 a new joint model is used. In this appendix a brief description of this model is presented.

A2 THEORY

Consider the joint between element i (lower numbered) and element j (higher numbered) (Fig. A1). In both elements vectors $\underline{t}$ en $\underline{f}$ are defined with the following properties:

$$(\underline{t}_i,\underline{t}_i) = (\underline{t}_j,\underline{t}_j) = (\underline{f}_i,\underline{f}_i) = (\underline{f}_j,\underline{f}_j) = 1$$
$$(\underline{t}_i,\underline{f}_i) = (\underline{t}_j,\underline{f}_j) = 0 \qquad \text{(A1)}$$

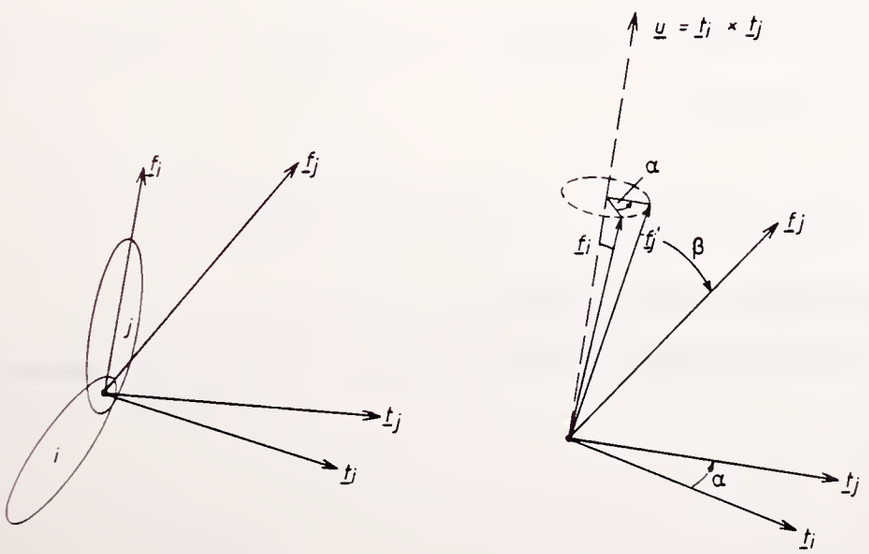

Fig. A1 Flexion-torsion model.

Two angles α and β will be defined to calculate the elastic torques. The angle α is defined as the angle between the vectors $\underline{t}_i$ and $\underline{t}_j$ and is called flexion angle:

$$\alpha = \arccos\ (A_i \underline{t}_i, A_j \underline{t}_j) \tag{A2}$$

where $0 \leqq \alpha < 180°$

$A_{i,j}$ = the (3*3) rotation matrices of element i and j

The rotation α is a rotation about the $\underline{u}$-axis, whereas the $\underline{u}$-vector is defined as:

$$\underline{u} = \frac{A_i \underline{t}_i \times A_j \underline{t}_j}{\left\| A_i \underline{t}_i \times A_j \underline{t}_j \right\|} \tag{A3}$$

As a consequence of the rotation α, the vector $\underline{f}_i$ takes the position $\underline{f}_j'$ as indicated in Fig. A1. The vector $\underline{f}_j'$ can be calculated by the following equation:

$$f_j' = (A_i \underline{f}_i, \underline{u}).\underline{u} + (A_i \underline{f}_i - \underline{u}(A_i \underline{f}_i, \underline{u})).\cos\alpha + (\underline{u} \times A_i \underline{f}_i).\ \sin\alpha \tag{A4}$$

The angle β will be defined as the rotation around the $\underline{t}_j$-axis, which transforms $\underline{f}_j'$ into $\underline{f}_j$ and is called the torsion angle. This angle can be calculated from:

$$\beta = \arccos\ (\underline{f}_j',\ A_j \underline{f}_j) \tag{A5}$$

The angle β can be either negative or positive. A direction of the rotation can be specified, namely,

if $((\underline{f}_j' \times A\underline{f}_j),\ A_j \underline{t}_j) < 0$ then β is negative.

The angle β is defined in the interval (-180,180).
The elastic torques are specified as function of α and β respectively:

$$M_f = f(\alpha) \tag{A6}$$
$$M_t = f(\beta)$$

where:

M_f = elastic torques for flexion,
M_t = elastic torques for torsion.

The flexion-torsion model calculates also a damping torque according to the following equation:

$$\underline{M}_d = -(\underline{b},\underline{v}) \tag{A7}$$

where:

$\underline{b}$ = damping coefficients in three directions

$\underline{v}$ = relative velocity for the calculation of the damping moment.

The relative velocity $\underline{v}$ consists of three mutually perpendicular components (Fig. 7):

$$\underline{v} = \begin{bmatrix} \alpha \\ \beta \\ \gamma \end{bmatrix} = \begin{bmatrix} (\underline{\omega},\underline{u}) \\ (\underline{\omega},A_j\underline{t}_j) \\ (\underline{\omega},A_j\underline{t}_j \times \underline{u}) \end{bmatrix} \tag{A8}$$

APENDIX B: Reprints of input data sets

Reprint of input data of two pivot model for frontal impact (DAMP2 REF1).

```
RUN  1
NST =  1
ST =  3  1
LBR =  3
NU =  3  2  1
GEO =  0.000  0.000  0.000  0.000  0.000  0.000
GEO =  0.000  0.000  0.000  0.000  0.000  0.063
GEO =  0.000  0.000  0.125  0.051  0.000  0.031
MA =   1.000E+03   1.000E+01   1.000E+01   1.000E+01
MA =   5.000E-01   5.000E-03   5.000E-03   1.000E+01
MA =   4.280E+00   2.300E-02   2.380E-02   1.205E-02
PCC =  0.0000  0.0000  0.0000   SCC =  0.0000  0.0000  0.0000
PCC =  0.0000  0.0000  0.0000   SCC =  0.0000  0.0000  0.0000
PCC =  0.0000  0.2444  0.0000   SCC =  0.0000  0.0000  0.0000
PCC =  0.0000 -0.6284  0.0000   SCC =  0.0000  0.0000  0.0000
TO = 0.00000   TS = 0.00100   TE = 0.30000
NJTQS =  0
NT =  2
TT  1=  1.  1.  2.  0.000  1.  0.  3.   0.00   0.00   0.00   0.00   0.00   0.00
        0.000  0.000  1.000 -0.242  0.000  0.970  1.000  0.000  0.000  0.970  0.000  0.242
TT  2=  1.  2.  3.  0.440  3.  2.  3.   0.00   1.00   0.00  10.00   0.00   0.00
        0.000  0.000  1.000  0.766  0.000  0.643  1.000  0.000  0.000  0.643  0.000 -0.766
KFSM =  3  RFSM =  5
FSM =     2.     2.     2.
FSM =  0.000  0.000  0.000
FSM =     0.     0.     0.
FSM =  1.000  1.000  1.000
FSM =   -72.  -500.     0.
RAMP1 = 0.100 RAMP2 = 1.000
ACC =  1  0  0
ACC =  0  0  2
ACC =  0  0  2
KFSA =  2  RFSA = 17
FSA =   8.000E+00   4.000E+00
FSA =   0.000E+00   0.000E+00
FSA =   0.000E+00   0.000E+00
FSA =   4.000E-02   4.900E-02
FSA =   0.000E+00   0.000E+00
FSA =   8.000E-02   5.000E-02
FSA =  -7.000E+01  -9.810E+00
FSA =   9.000E-02   1.000E+00
FSA =  -1.150E+02  -9.810E+00
FSA =   1.100E-01   0.000E+00
FSA =  -9.000E+01   0.000E+00
FSA =   1.500E-01   0.000E+00
FSA =  -1.000E+02   0.000E+00
FSA =   2.600E-01   0.000E+00
FSA =   0.000E+00   0.000E+00
FSA =   3.000E-01   0.000E+00
FSA =   0.000E+00   0.000E+00
NET =  3
ET   1=  1.  1.  0.075  0.150  0.150  0.000  0.000 -0.130  2.  0.000
ET   2=  1.  2.  0.050  0.050  0.075  0.000  0.000  0.062  2.  0.000
ET   3=  1.  3.  0.075  0.075  0.100  0.019  0.000  0.020  2.  0.000
NPLT =  1
PLT  1=  0.  0.  0.000  0.000  0.000  0.000  0.000  0.000  0.000  0.000  0.000  0.000  0.000  0.000
NBT =  0
```

Reprint of input data of two pivot model for lateral impact (REF2)

```
RUN  2
NST =  1
ST =  3  1
LBR =  3
NU =  3  2  1
GEO =  0.000  0.000  0.000  0.000  0.000  0.000
GEO =  0.000  0.000  0.000  0.000  0.000  0.063
GEO =  0.000  0.000  0.125  0.051  0.000  0.031
MA =   1.000E+03   1.000E+01   1.000E+01   1.000E+01
MA =   5.000E-01   5.000E-03   5.000E-03   1.000E+01
MA =   4.280E+00   2.300E-02   2.380E-02   1.235E-02
PCC =  0.0000  0.0000  0.0000   SCC =  0.0000  0.0000  0.0000
PCC =  0.0000  0.0000  1.5707   SCC =  0.0000  0.0000  0.0000
PCC =  0.0000  0.0873  1.5707   SCC =  0.0000  0.0000  0.0000
PCC =  0.6283  0.0000  1.5707   SCC =  0.0000  0.0000  0.0000
TO = 0.00000   TS = 0.00100   TE = 0.30000
NJTQS =  0
NT =  2
TT  1=  1.  1.  2.  0.000  1.  0.  3.   0.00   0.00   0.00   0.00   0.00   0.00
        0.000  0.000  1.000  0.000  0.087  0.996  1.000  0.000  0.000  1.000  0.000  0.000
TT  2=  1.  2.  3.  0.175  3.  2.  4.   0.00   1.00   0.00  10.00   0.00   0.00
        0.000  0.000  1.000  0.586 -0.087  0.806  1.000  0.000  0.000  0.809  0.000 -0.588
KFSM =  4  RFSM =  5
FSM =     2.     2.     2.     2.
FSM =  0.000  0.000  0.000  0.000
FSM =     0.     0.     0.     0.
FSM =  1.000  1.000  1.000  1.000
FSM =   -86.  -500.     0.   -14.
RAMP1 = 0.100 RAMP2 = 1.000
ACC =  1  0  0
ACC =  0  0  2
ACC =  0  0  2
KFSA =  2  RFSA = 23
FSA =   1.100E+01   4.000E+00
FSA =   0.000E+00   0.000E+00
FSA =   0.000E+00   0.000E+00
FSA =   5.200E-02   7.900E-02
FSA =   0.000E+00   0.000E+00
FSA =   8.200E-02   8.000E-02
FSA =  -2.500E+01  -9.810E+00
FSA =   9.400E-02   1.000E+00
FSA =  -1.050E+02  -9.810E+00
FSA =   1.090E-01   0.000E+00
FSA =  -1.000E+02   0.000E+00
FSA =   1.200E-01   0.000E+00
FSA =  -4.500E+01   0.000E+00
FSA =   1.460E-01   0.000E+00
FSA =  -6.500E+01   0.000E+00
FSA =   1.710E-01   0.000E+00
FSA =  -1.500E+01   0.000E+00
FSA =   1.960E-01   0.000E+00
FSA =  -5.000E+01   0.000E+00
FSA =   2.600E-01   0.000E+00
FSA =   0.000E+00   0.000E+00
FSA =   3.000E-01   0.000E+00
FSA =   0.000E+00   0.000E+00
NET =  3
ET   1=  1.  1.  0.075  0.150  0.150  0.000  0.000 -0.130  2.  0.000
ET   2=  1.  2.  0.050  0.050  0.075  0.000  0.000  0.062  2.  0.000
ET   3=  1.  3.  0.075  0.075  0.100  0.019  0.000  0.020  2.  0.000
NPLT =  1
PLT  1=  0.  0.  0.000  0.000  0.000  0.000  0.000  0.000  0.000  0.000  0.000  0.000  0.000  0.000
NBT =  0
```

Reprint of input data of two pivot model for oblique impact (REF3)

```
RUN  3
NST =  1
ST =  3  1
LBR =  3
NU =  3  2  1
GEO =  0.000  0.000  0.000  0.000  0.000  0.000
GEO =  0.000  0.000  0.000  0.000  0.000  0.063
GEO =  0.000  0.000  0.125  0.051  0.000  0.031
MA =   1.000E+03   1.000E+01   1.000E+01   1.000E+01
MA =   5.000E-01   5.000E-03   5.000E-03   1.000E+01
MA =   4.280E+00   2.300E-02   2.380E-02   1.235E-02
PCC =  0.0000  0.0000  0.0000   SCC =  0.0000  0.0000  0.0000
PCC =  0.0000  0.0000  0.7854   SCC =  0.0000  0.0000  0.0000
PCC =  0.0000  0.1746  0.7854   SCC =  0.0000  0.0000  0.0000
PCC =  0.4746 -0.4286  0.8906   SCC =  0.0000  0.0000  0.0000
TO = 0.00000   TS = 0.00100   TE = 0.30000
NJTQS =  0
NT =  2
TT  1=  1.  1.  2.  0.000  1.  0.  3.   0.00   0.00   0.00   0.00   0.00   0.00
        0.000  0.000  1.000 -0.123  0.123  0.985  1.000  0.000  0.000  0.992  0.008  0.123
TT  2=  1.  2.  3.  0.350  3.  2.  4.   0.00   1.00   0.00  10.00   0.00   0.00
        0.000  0.000  1.000  0.678 -0.123  0.725  1.000  0.000  0.000  0.731  0.008 -0.683
KFSM =  4  RFSM =  5
FSM =     2.     2.     2.     2.
FSM =  0.000  0.000  0.000  0.000
FSM =     0.     0.     0.     0.
FSM =  1.000  1.000  1.000  1.000
FSM =   -72.  -500.     0.   -29.
RAMP1 = 0.100 RAMP2 = 1.000
ACC =  1  0  0
ACC =  0  0  2
ACC =  0  0  2
KFSA =  2  RFSA = 17
FSA =   8.000E+00   4.000E+00
FSA =   0.000E+00   0.000E+00
FSA =   0.000E+00   0.000E+00
FSA =   5.000E-02   6.300E-02
FSA =   0.000E+00   0.000E+00
FSA =   6.400E-02   6.400E-02
FSA =  -2.500E+01  -9.810E+00
FSA =   8.600E-02   1.000E-01
FSA =  -1.100E+02  -9.810E+00
FSA =   9.800E-02   0.000E+00
FSA =  -1.200E+02   0.000E+00
FSA =   1.320E-01   0.000E+00
FSA =  -6.500E+01   0.000E+00
FSA =   2.200E-01   0.000E+00
FSA =   0.000E+00   0.000E+00
FSA =   3.000E-01   0.000E+00
FSA =   0.000E+00   0.000E+00
NET =  3
ET   1=  1.  1.  0.075  0.250  0.150  0.000  0.000 -0.130  2.  0.000
ET   2=  1.  2.  0.050  0.050  0.075  0.000  0.000  0.062  2.  0.000
ET   3=  1.  3.  0.075  0.075  0.100  0.019  0.000  0.020  2.  0.000
NPLT =  1
PLT  1=  0.  0.  0.000  0.000  0.000  0.000  0.000  0.000  0.000  0.000  0.000  0.000  0.000  0.000
N8T =  0
```

Reprint of input data of model of Part 572 (sled)

```
RUN  1
NST =  1
ST =  8  1
LBR =  8
NU =  8  7  6  5  4  3  2  1
GEO =  0.000  0.000  0.000  0.000
GEO =  0.000  0.000  0.000  0.008
GEO =  0.000  0.016  0.000  0.008
GEO =  0.000  0.016  0.000  0.008
GEO =  0.000  0.016  0.000  0.008
GEO =  0.000  0.016  0.000  0.008
GEO =  0.000  0.016  0.000  0.008
GEO =  0.000  0.016  0.006  0.043
MA =  1.000E+03  1.000E+01
MA =  1.250E-01  1.000E-03
MA =  1.250E-01  1.000E-03
MA =  1.250E-01  1.000E-03
MA =  1.250E-01  1.000E-03
MA =  1.250E-01  1.000E-03
MA =  1.250E-01  1.000E-03
MA =  4.480E+00  3.070E-02
PCC =  0.0000   SCC =  0.0000
PCC =  0.0000   SCC =  0.0000
PCC =  0.0000   SCC =  0.0000
PCC = -0.3500   SCC =  0.0000
PCC = -0.3500   SCC =  0.0000
PCC = -0.3500   SCC =  0.0000
PCC = -0.3500   SCC =  0.0000
PCC = -0.3500   SCC =  0.0000
PCC = -0.3500   SCC =  0.0000
PCC = -0.3500   SCC =  0.0000
TO = 0.00000   TS = 0.00100   TE = 0.15000
MAXF = 20  MAXM =  7
NJTQS =  7
MT  1=  1.  1.  2.  2.  0.750  0.000  0.000  0.000
MT  2=  1.  2.  3.  1.  0.750  0.000  0.000  0.000
MT  3=  1.  3.  4.  1.  0.750  0.000  0.000  0.000
MT  4=  1.  4.  5.  1.  0.750  0.000  0.000  0.000
MT  5=  1.  5.  6.  1.  0.750  0.000  0.000  0.000
MT  6=  1.  6.  7.  1.  0.750  0.000  0.000  0.000
MT  7=  1.  7.  8.  1.  0.750  0.000  0.000  0.000
KFSM =  2  RFSM =  7
FSM =  3.000E+00  3.000E+00
FSM = -1.000E+00 -1.350E+00
FSM =  5.230E+02  5.230E+02
FSM =  0.000E+00 -3.500E-01
FSM =  0.000E+00  0.000E+00
FSM =  1.000E+00  6.500E-01
FSM = -5.230E+02 -5.230E+02
ACC =  1  0
ACC =  0  2
ACC =  0  2
ACC =  0  2
ACC =  0  2
ACC =  0  2
ACC =  0  2
ACC =  0  2
KFSA =  2  RFSA = 17
FSA =  8.000E+00  4.000E+00
FSA =  0.000E+00  0.000E+00
FSA =  0.000E+00  0.000E+00
FSA =  3.000E-02  3.000E-02
FSA =  0.000E+00  0.000E+00
FSA =  7.500E-02  3.100E-02
FSA = -3.350E+02 -9.810E+00

FSA =  8.900E-02  1.000E+00
FSA = -3.450E+02 -9.810E+00
FSA =  9.800E-02  0.000E+00
FSA = -3.300E+02  0.000E+00
FSA =  1.290E-01  0.000E+00
FSA = -1.650E+02  0.000E+00
FSA =  1.470E-01  0.000E+00
FSA =  0.000E+00  0.000E+00
FSA =  2.000E-01  0.000E+00
FSA =  0.000E+00  0.000E+00
NET =  0
NBT =  0
```

Reprint of input data of first CAD model (CAD1)

```
RUN  1
NST =  1
ST =  8  1
LBR =  8
NU =  8  7  6  S  4  3  2  1
GEO =  0.000  0.000  0.000  0.000
GEO =  0.000  0.000  0.000  0.008
GEO =  0.000  0.016  0.000  0.008
GEO =  0.000  0.016  0.000  0.008
GEO =  0.000  0.016  0.000  0.008
GEO =  0.000  0.016  0.000  0.008
GEO =  0.000  0.016  0.000  0.008
GEO =  0.000  0.016  0.006  0.043
MA =  1.000E+03  1.000E+01
MA =  1.250E-01  1.000E-03
MA =  1.250E-01  1.000E-03
MA =  1.250E-01  1.000E-03
MA =  1.250E-01  1.000E-03
MA =  1.250E-01  1.000E-03
MA =  1.250E-01  1.000E-03
MA =  4.480E+00  3.070E-02
PCC =  0.0000   SCC =  0.0000
PCC =  0.0000   SCC =  0.0000
PCC =  0.0000   SCC =  0.0000.
PCC = -0.3S00   SCC =  0.0000
PCC = -0.3S00   SCC =  0.0000
PCC = -0.3S00   SCC =  0.0000
PCC = -0.3S00   SCC =  0.0000
PCC = -0.3S00   SCC =  0.0000
PCC = -0.3S00   SCC =  0.0000
PCC =  0.0000   SCC =  0.0000
TO = 0.00000   TS = 0.00100   TE = 0.30000
MAXF = 20  MAXM =  7
NJTQS =  7
MT  1=  1.  1.  2.  2.  0.7S0  0.000  0.000  0.000
MT  2=  1.  2.  3.  1.  0.75U  0.000  0.000  0.000
MT  3=  1.  3.  4.  1.  0.7S0  0.000  0.000  0.000
MT  4=  1.  4.  S.  1.  0.7S0  0.000  0.000  0.000
MT  5=  1.  5.  6.  1.  0.750  0.000  0.000  0.000
MT  6=  1.  6.  7.  1.  0.7S0  0.000  0.000  0.000
MT  7=  1.  7.  8.  3.  0.750  0.000  0.000  0.000
KFSM =  3  RFSM =  7
FSM =   3.000E+00   3.000E+00   3.000E+00
FSM =  -1.000E+00  -1.350E+00  -6.S00E-01
FSM =   2.600E+02   2.600E+02   2.600E+02
FSM =   0.000E+00  -3.S00E-01   3.S00E-01
FSM =   0.000E+00   0.000E+00   0.000E+00
FSM =   1.000E+00   6.500E-01   1.350E+00
FSM =  -2.600E+02  -2.600E+02  -2.600E+02
ACC =  1  0
ACC =  0  2
ACC =  0  2
ACC =  0  2
ACC =  0  2
ACC =  0  2
ACC =  0  2
ACC =  0  2
KFSA =  2  RFSA = 21
FSA =  1.000E+01  4.000E+00
FSA =  0.000E+00  0.000E+00
FSA =  0.000E+00  0.000E+00
FSA =  4.000E-02  4.900E-02
FSA =  0.000E+00  0.000E+00
FSA =  8.200E-02  S.000E-02
FSA = -1.400E+02 -9.810E+00

FSA =  1.000E-01  1.000E+00
FSA = -1.100E+02 -9.810E+00
FSA =  1.060E-01  0.000E+00
FSA = -1.900E+02  0.000E+00
FSA =  1.120E-01  0.000E+00
FSA = -1.900E+02  0.000E+00
FSA =  1.1S0E-01  0.000E+00
FSA = -1.2S0E+02  0.000E+00
FSA =  1.400E-01  0.000E+00
FSA = -1.500E+02  0.000E+00
FSA =  2.2S0E-01  0.000E+00
FSA =  0.000E+00  0.000E+00
FSA =  2.800E-01  0.000E+00
FSA =  0.000E+00  0.000E+00
NET =  0
NBT =  0
```

Reprint of input data of second CAD model (CAD2)

```
RUN  2
NST =  1
ST =  8  1
LBR =  8
NU =  8  7  6  5  4  3  2  1
GEO =  0.000  0.000  0.000  0.000
GEO =  0.000  0.000  0.000  0.008
GEO =  0.000  0.016  0.000  0.008
GEO =  0.000  0.016  0.000  0.008
GEO =  0.000  0.016  0.000  0.008
GEO =  0.000  0.016  0.000  0.008
GEO =  0.000  0.016  0.000  0.008
GEO =  0.000  0.016  0.006  0.043
MA =  1.000E+03  1.000E+01
MA =  1.250E-01  1.000E-03
MA =  1.250E-01  1.000E-03
MA =  1.250E-01  1.000E-03
MA =  1.250E-01  1.000E-03
MA =  1.250E-01  1.000E-03
MA =  1.250E-01  1.000E-03
MA =  4.480E+00  3.070E-02
PCC =  0.0000   SCC =  0.0000
PCC =  0.0000   SCC =  0.0000
PCC =  0.0000   SCC =  0.0000
PCC = -0.3500   SCC =  0.0000
PCC = -0.3500   SCC =  0.0000
PCC = -0.3500   SCC =  0.0000
PCC = -0.3500   SCC =  0.0000
PCC = -0.3500   SCC =  0.0000
PCC = -0.3500   SCC =  0.0000
PCC =  0.0000   SCC =  0.0000
TO = 0.00000   TS = 0.00100   TE = 0.30000
MAXF = 20  MAXM =  7
NJTQS =  7
MT  1=  1.  1.  2.  2.  0.750  0.000  0.000  0.000
MT  2=  1.  2.  3.  1.  0.750  0.000  0.000  0.000
MT  3=  1.  3.  4.  1.  0.750  0.000  0.000  0.000
MT  4=  1.  4.  5.  1.  0.750  0.000  0.000  0.000
MT  5=  1.  5.  6.  1.  0.750  0.000  0.000  0.000
MT  6=  1.  6.  7.  1.  0.750  0.000  0.000  0.000
MT  7=  1.  7.  8.  3.  0.750  0.000  0.000  0.000
KFSM =  3  RFSM =  7
FSM =   3.000E+00   3.000E+00   2.000E+00
FSM =  -1.000E+00  -1.350E+00   0.000E+00
FSM =   2.600E+02   2.600E+02   0.000E+00
FSM =   0.000E+00  -3.500E-01   1.000E+00
FSM =   0.000E+00   0.000E+00  -1.000E+03
FSM =   1.000E+00   6.500E-01   0.000E+00
FSM =  -2.600E+02  -2.600E+02   0.000E+00
ACC =  1  0
ACC =  0  2
ACC =  0  2
ACC =  0  2
ACC =  0  2
ACC =  0  2
ACC =  0  2
ACC =  0  2
KFSA =  2  RFSA = 21
FSA =  1.000E+01  4.000E+00
FSA =  0.000E+00  0.000E+00
FSA =  0.000E+00  0.000E+00
FSA =  4.000E-02  4.900E-02
FSA =  0.000E+00  0.000E+00
FSA =  8.200E-02  5.000E-02
FSA = -1.400E+02 -9.810E+00

FSA =  1.000E-01  1.000E+00
FSA = -1.100E+02 -9.810E+00
FSA =  1.060E-01  0.000E+00
FSA = -1.900E+02  0.000E+00
FSA =  1.120E-01  0.000E+00
FSA = -1.900E+02  0.000E+00
FSA =  1.150E-01  0.000E+00
FSA = -1.250E+02  0.000E+00
FSA =  1.400E-01  0.000E+00
FSA = -1.500E+02  0.000E+00
FSA =  2.250E-01  0.000E+00
FSA =  0.000E+00  0.000E+00
FSA =  2.800E-01  0.000E+00
FSA =  0.000E+00  0.000E+00
NET =  0
NBT =  0
```

Reprint of input data of third CAD model (CAD3)

```
RUN  3
NST =  1
ST = 13  1
LBR = 13
NU = 13 12 11 10  9  8  7  6  5  4
NU =  3  2  1
GEO =  0.000  0.000  0.000  0.000
GEO =  0.000  0.000  0.000  0.008
GEO =  0.000  0.016  0.000  0.008
GEO =  0.000  0.016  0.000  0.008
GEO =  0.000  0.016  0.000  0.008
GEO =  0.000  0.016  0.000  0.008
GEO =  0.000  0.016  0.000  0.008
GEO =  0.000  0.016  0.000  0.008
GEO =  0.000  0.016  0.000  0.008
GEO =  0.000  0.016  0.000  0.008
GEO =  0.000  0.016  0.000  0.008
GEO =  0.000  0.016 -0.013 -0.035
MA =  1.000E+03  1.000E+01
MA =  1.250E-01  1.000E-03
MA =  1.250E-01  1.000E-03
MA =  1.250E-01  1.000E-03
MA =  1.250E-01  1.000E-03
MA =  1.250E-01  1.000E-03
MA =  1.250E-01  1.000E-03
MA =  1.250E-01  1.000E-03
MA =  1.250E-01  1.000E-03
MA =  1.250E-01  1.000E-03
MA =  1.250E-01  1.000E-03
MA =  1.250E-01  1.000E-03
MA =  4.480E+00  3.070E-02
PCC =  0.0000   SCC =  0.0000
PCC =  0.0000   SCC =  0.0000
PCC =  0.0000   SCC =  0.0000
PCC = -0.3500   SCC =  0.0000
PCC = -0.3500   SCC =  0.0000
PCC = -0.3500   SCC =  0.0000
PCC = -0.3500   SCC =  0.0000
PCC = -0.3500   SCC =  0.0000
PCC = -0.3500   SCC =  0.0000
PCC = -0.3500   SCC =  0.0000
PCC = -0.3500   SCC =  0.0000
PCC = -0.3500   SCC =  0.0000
PCC = -0.3500   SCC =  0.0000
PCC = -0.3500   SCC =  0.0000
PCC =  0.0000   SCC =  0.0000
TO = 0.00000   TS = 0.00100   TE = 0.30000
MAXF = 20  MAXM = 12
NJTQS = 12
MT  1=  1.  1.  2.  2.  0.750  0.000  0.000  0.000
MT  2=  1.  2.  3.  1.  0.750  0.000  0.000  0.000
MT  3=  1.  3.  4.  1.  0.750  0.000  0.000  0.000
MT  4=  1.  4.  5.  1.  0.750  0.000  0.000  0.000
MT  5=  1.  5.  6.  1.  0.750  0.000  0.000  0.000
MT  6=  1.  6.  7.  1.  0.750  0.000  0.000  0.000
MT  7=  1.  7.  8.  1.  0.750  0.000  0.000  0.000
MT  8=  1.  8.  9.  1.  0.750  0.000  0.000  0.000
MT  9=  1.  9. 10.  1.  0.750  0.000  0.000  0.000
MT 10=  1. 10. 11.  1.  0.750  0.000  0.000  0.000
MT 11=  1. 11. 12.  1.  0.750  0.000  0.000  0.000
MT 12=  1. 12. 13.  3.  0.750  0.000  0.000  0.000
KFSM =  3  RFSM =  7
FSM =   3.000E+00   3.000E+00   3.000E+00
FSM =  -1.000E+00  -1.350E+00  -6.500E-01
FSM =   2.600E+02   2.600E+02   2.600E+02
FSM =   0.000E+00  -3.500E-01   3.500E-01
FSM =   0.000E+00   0.000E+00   0.000E+00
FSM =   1.000E+00   6.500E-01   1.350E+00
FSM =  -2.600E+02  -2.600E+02  -2.600E+02
ACC =  1  0
ACC =  0  2
ACC =  0  2
ACC =  0  2
ACC =  0  2
ACC =  0  2
ACC =  0  2
ACC =  0  2
ACC =  0  2
ACC =  0  2
ACC =  0  2
ACC =  0  2
KFSA =  2  RFSA = 21
FSA =  1.000E+01  4.000E+00
FSA =  0.000E+00  0.000E+00
FSA =  0.000E+00  0.000E+00
FSA =  4.000E-02  4.900E-02
FSA =  0.000E+00  0.000E+00
FSA =  8.200E-02  5.000E-02
FSA = -1.400E+02 -9.810E+00
FSA =  1.000E-01  1.000E+00
FSA = -1.100E+02 -9.810E+00
FSA =  1.060E-01  0.000E+00
FSA = -1.900E+02  0.000E+00
FSA =  1.120E-01  0.000E+00
FSA = -1.900E+02  0.000E+00
FSA =  1.150E-01  0.000E+00
FSA = -1.250E+02  0.000E+00
FSA =  1.400E-01  0.000E+00
FSA = -1.500E+02  0.000E+00
FSA =  2.250E-01  0.000E+00
FSA =  0.000E+00  0.000E+00
FSA =  2.800E-01  0.000E+00
FSA =  0.000E+00  0.000E+00
NET =  0
N8T =  0
```

Reprint of input data of fourth CAD model (CAD4)

```
RUN  4
NST =  1
ST =  8  1
LBR =  8
NU =  8  7  6  5  4  3  2  1
GEO =  0.000  0.000  0.000  0.000
GEO =  0.000  0.000  0.000  0.008
GEO =  0.000  0.016  0.000  0.008
GEO =  0.000  0.016  0.000  0.008
GEO =  0.000  0.016  0.000  0.008
GEO =  0.000  0.016  0.000  0.008
GEO =  0.000  0.016  0.000  0.008
GEO =  0.000  0.016  0.006  0.043
MA =  1.000E+03  1.000E+01
MA =  1.250E-01  1.000E-03
MA =  1.250E-01  1.000E-03
MA =  1.250E-01  1.000E-03
MA =  1.250E-01  1.000E-03
MA =  1.250E-01  1.000E-03
MA =  1.250E-01  1.000E-03
MA =  4.480E+00  3.070E-02
PCC =  0.0000   SCC =  0.0000
PCC =  0.0000   SCC =  0.0000
PCC =  0.0000   SCC =  0.0000
PCC = -0.3500   SCC =  0.0000
PCC = -0.3500   SCC =  0.0000
PCC = -0.3500   SCC =  0.0000
PCC = -0.3500   SCC =  0.0000
PCC = -0.3500   SCC =  0.0000
PCC = -0.3500   SCC =  0.0000
PCC =  0.0000   SCC =  0.0000
TO = 0.00000   TS = 0.00100   TE = 0.30000
MAXF = 20  MAXM =  7
NJTQS =  7
MT  1=  1.  1.  2.  2.  0.750  0.000  0.000  0.000
MT  2=  1.  2.  3.  1.  0.750  0.000  0.000  0.000
MT  3=  1.  3.  4.  1.  0.750  0.000  0.000  0.000
MT  4=  1.  4.  5.  1.  0.750  0.000  0.000  0.000
MT  5=  1.  5.  6.  1.  0.750  0.000  0.000  0.000
MT  6=  1.  6.  7.  1.  0.750  0.000  0.000  0.000
MT  7=  1.  7.  8.  3.  0.750  0.000  0.000  0.000
KFSM =  3  RFSM =  7
FSM =   3.000E+00   3.000E+00   3.000E+00
FSM =  -1.000E+00  -1.350E+00  -6.500E-01
FSM =   6.000E+01   6.000E+01   6.000E+01
FSM =   0.000E+00  -3.500E-01   3.500E-01
FSM =   0.000E+00   0.000E+00   0.000E+00
FSM =   1.000E+00   6.500E-01   1.350E+00
FSM =  -6.000E+01  -6.000E+01  -6.000E+01
ACC =  1  0
ACC =  0  2
ACC =  0  2
ACC =  0  2
ACC =  0  2
ACC =  0  2
ACC =  0  2
ACC =  0  2
KFSA =  2  RFSA = 21
FSA =  1.000E+01  4.000E+00
FSA =  0.000E+00  0.000E+00
FSA =  0.000E+00  0.000E+00
FSA =  4.000E-02  4.900E-02
FSA =  0.000E+00  0.000E+00
FSA =  8.200E-02  5.000E-02
FSA = -1.400E+02 -9.810E+00

FSA =  1.000E-01  1.000E+00
FSA = -1.100E+02 -9.810E+00
FSA =  1.060E-01  0.000E+00
FSA = -1.900E+02  0.000E+00
FSA =  1.120E-01  0.000E+00
FSA = -1.900E+02  0.000E+00
FSA =  1.150E-01  0.000E+00
FSA = -1.250E+02  0.000E+00
FSA =  1.400E-01  0.000E+00
FSA = -1.500E+02  0.000E+00
FSA =  2.250E-01  0.000E+00
FSA =  0.000E+00  0.000E+00
FSA =  2.800E-01  0.000E+00
FSA =  0.000E+00  0.000E+00
NET =  0
NBT =  2
BT =   1.  8. -0.020  0.000  1.  1. -0.020  0.000  0.000  1.
BT =   1.  8.  0.020  0.000  1.  1.  0.020  0.000  0.000  1.
SPRINGLENGTHS =  0.095  0.095
NBTA =  0
KFSB =  1  RFSB =  5
FSB =  2.000E+00
```

APENDIX C

COMPARISON OF MASS DISTRIBUTION DATA OF THE PART 572 DUMMY AND RECOMMENDATIONS FOR A STANDARD DATASET FOR CVS MODELING*

Jac Wismans,
Research Institute for Road Vehicles TNO,
Delft, The Netherlands

Introduction

Crash Victim Simulations (CVS) models most frequently used now in the field of automotive safety are MVMA[1], CALSPAN[2] and MADYMO[3]. Datasets used in these computer programs to represent the 50% Part 572 dummy appear to be not completely identical. These differences are mainly due to differences in:

- segment division
- number of segments used to describe the dummy
- location of segment coordinate systems
- methods used to measure dummy characteristics
- the dummies selected for the measurement of the dummy characteristics
- program features like e.g. for the description of joint characteristics

In addition some dummy characteristics are hard to measure or cannot be measured at all. Also the type of simulation, i.e. frontal versus side or pedestrian impact, restrained versus unrestrained, 2D versus 3D etc. can effect the representation of the dummy.

---

* This document has been prepared for the Analytical Human Simulation Task Force of the SAE Human Biomechanics and Simulation Subcommittee (aug. 1983). Comments and suggestions can be sent to the chairman of this Task Force: dr. Priyaranjan Prasad, Ford Motor Company, Automotive Safety Center, P.O. Box 253, Dearborn, Mi 48221, USA.

An analysis will be presented here of Part 572 dummy mass distribution data based on measurements conducted at three different laboratories:

- "Hubbard" presented in Reference (4).
- "Calspan" presented in Volume 2 of Reference (2).
- "TNO" presented in Reference (5).

"Hubbard" data don't include 3-dimensional moments of inertia and are used in datasets for frontal impacts of MVMA and the MADYMO 2-dimensional version. "Calspan" data are used in the CALSPAN model and "TNO" data in the MADYMO 3-dimensional version. Mass distribution data to be presented here include masses, moments of inertia, center of gravity location and distances between pivots.

On the basis of this analysis, a standard mass distribution dataset will be proposed derived from these three sources. This dataset will be extended in future with joint characteristics and body stiffness data.

Division in Segments

In order to measure mass distribution data, the dummy has to be divided into a number of segments. The segment division used by the three laboratories is not completely identical which makes it more difficult to compare in a direct way the results of these laboratories. In this study, a division in 13 segments is proposed: head, neck, upper torso, center torso, lower torso, upper arms, lower arms and hands, upper legs, lower legs and feet. The center torso has 2 parts:lumbar spine and abdominal insert. Figure 1 shows roughly which components belong to a segment. Bolts and other small components are not separately assigned to a segment here, since difference methods are used in the three studies. The effects of this is expected to be small. Further it is assumed that no instrumentation is included in the dummy segments. Table 1 summarizes the deviations between the segment division used in this study and the ones used by the laboratories.

The standard dataset for a 3-dimensional representation of the dummy in a mathematical model, proposed here, will be based on a similar division in 13

segments. A corresponding dataset for a 2-dimensional representation simply can be derived from this proposed 3-dimensional dataset and would consist of 13 segments in case of side impacts, and 9 segments in case of frontal impacts.

Segment coordinate systems

For each segment, a right-handed coordinate system x, y, z is defined. In a standing upright position with the arms down and the legs straight, all z-axis are in the upward direction, all x-axis are forward and all y-axis are to the left (see Figure 2). The location of the local coordinate systems is indicated in Figure 1 and specified in more detail in Table 2.

The origins of the coordinate systems are selected in joint centers of rotation as far as the limbs are concerned and in the center of the endplanes of the rubber cylinders representing neck and spine, for the other segments.

Since in the dummy the neck centerline is rotated 20 degrees forward relative to the spine centerline (2), the head and neck local coordinate systems are rotated 20 degrees with respect to the upper torso cordinate system (if no forces are applied on the head/neck structure). In the reference position (standing) illustrated in Figure 2, all other segment coordinate systems have the same orientation.

Mass distribution data

In this section, data from the three sources are compared with each other. Where possible, additional calculations are made in order to have the data expressed in agreement with the preceding segment and coordinate system definitions.

Both CALSPAN and TNO data are based on measurements of one dummy (Alderson) while the data presented by Hubbard relate to two dummies by different manufacturers (Alderson and Sierra). Average values will be presented here if separate measurements for the left and right segments were conducted.

Table 3 shows a comparison of measured segment masses. The largest difference appears to be in the lower torso mass which is 1.6 kg higher in the Sierra dummy (Hubbard) than in the Alderson dummy (TNO). Differences in mass for the other segments are smaller than 0.5 kg.

Results for the center of gravity measurements are shown in Table 4. Values between -5 and +5 mm are neglected in this table. It turns out that except for the upper leg, all centers of gravity are located in the (x,z)-plane of the segment. It should be noted that results of the CALSPAN measurements for the lower torso and the upper leg cannot be compared with the other sources due to different segment definitions. Differences in center of gravity locations between various measurements are found to be relatively small. Largest differences (i.e. 3 cm) appear to be in the x-coordinate of the abdominal insert.

Table 5 summarizes the segment principal moments of inertia. Only Hubbard conducted measurements about the local y-axis. In the TNO measurements, the axis of the local coordinate systems were assumed to have the same orientation as the principal axis. According to the measurements of CALSPAN, this appears to be a reasonable approximation for most of the dummy segments. Significant differences between both axis systems were noted only for the head and the lower torso as indicated in Table 5 (note 4 and note 7).

Like for the center of gravity measurements, CALSPAN moments of inertia for the lower torso and upper leg cannot be compared with the results of the other laboratories due to differences in segment definition. The same holds for the upper torso measurements by TNO, which were based on another segment definition (i.e. without shoulders). The deviations between moment of inertia are, in general, less than 20%, except for smaller segments (i.e. spine and neck) and for moments of inertia about the longitudinal axis of slender elements (limbs). In the case of the neck and spine, calculated values (CALSPAN/TNO) are expected to be more accurate than measured ones (Hubbard).

Table 6 presents the positions of the origins of the segment coordinate systems expressed in the coordinates of an adjoining element. For the limbs, the origins are taken identical to joint centers of rotation. For the torso,

head and neck segments, no unique pivots can be defined due to the flexible spine and neck structures. It will be assumed here that these joints can be reasonably located on the centerlines in the endplanes of the rubber cylinders so coinciding with origins of torso, neck and head segments. Thus, this table implicitly presents the joint locations (and link length). Data provided by TNO are based on measurements from the assembly drawings, so are expected to be less accurate. Measured data by Calspan and Hubbard only show significant differences for the shoulder (0.03 m) and for the knee (0.01 m). With respect to the shoulder, this most likely will be due to differences in defining the reference position of the shoulder with respect to the torso.

Recommendation for a dataset (mass distribution)

Based on the preceding analysis, a dataset will be proposed here which can be used for 3-dimensional CVS models. This dataset is presented in Table 7 (mass and moments of inertia), Table 8 (center of gravity) and Table 9 (joint location). The dataset only holds for a division of the dummy in 13 segments and for a segment and coordinate system definition as proposed in this study (see Figure 1-2 and Table 1, 2). Footnotes in the tables describe in what way the data were obtained.

In this way the complete mass distribution of the Part 572 dummy is defined. It should be noted here that:

- in a standing position of the dummy (see Figure 2) all local coordinates except for the head and the neck have the same orientation. The neck and head local coordinates system are rotated forward 20^{o} with respect to the torso local coordinate system.

- all local principal axis except for the head are assumed to have the same orientation as the proposed local coordinate systems. For the head the principal axis system is taken -43 degrees rotated about the y-axis of the local head coordinate system (i.e. rotated backwards).

References

1. Bowman, B.M., Bennett, R.O., Robbins, D.H. (1979): "MVMA Two-dimensional Crash Victim Simulation, Version 4" Vol. 1,2,3. Final Report UM HSRI 79-5.

2. Fleck, J.T., Butler, F.E. and DeLeys, N.J. (1982): "Validation of the Crash Victim Simulator" Vol. 1,2,3,4. Report No 25 5881-V, Calspan, Buffalo, N.Y.

3. Wismans, J., Maltha, J., van Wijk, J.J. and Janssen, E.G. (1982): "MADYMO - A Crash Victim Simulation Program for Biomechanical Research and Optimization of Designs for Impact Injury Prevention". AGARD Conference Proceeding No 322.

4. Hubbard, R.P. and McLead, D.G. (1977): Geometric, Inertial and Joint Characteristics of Two Part 572 Dummies for Occupant Modeling. 21st Stapp Conference.

5. Hasselman, J. (1980): Drie-dimensionale Dummiekarakteristieken t.b.v. MADYMO - Computersimulaties. Report 700120002-H, IW-TNO, Delft, The Netherlands.

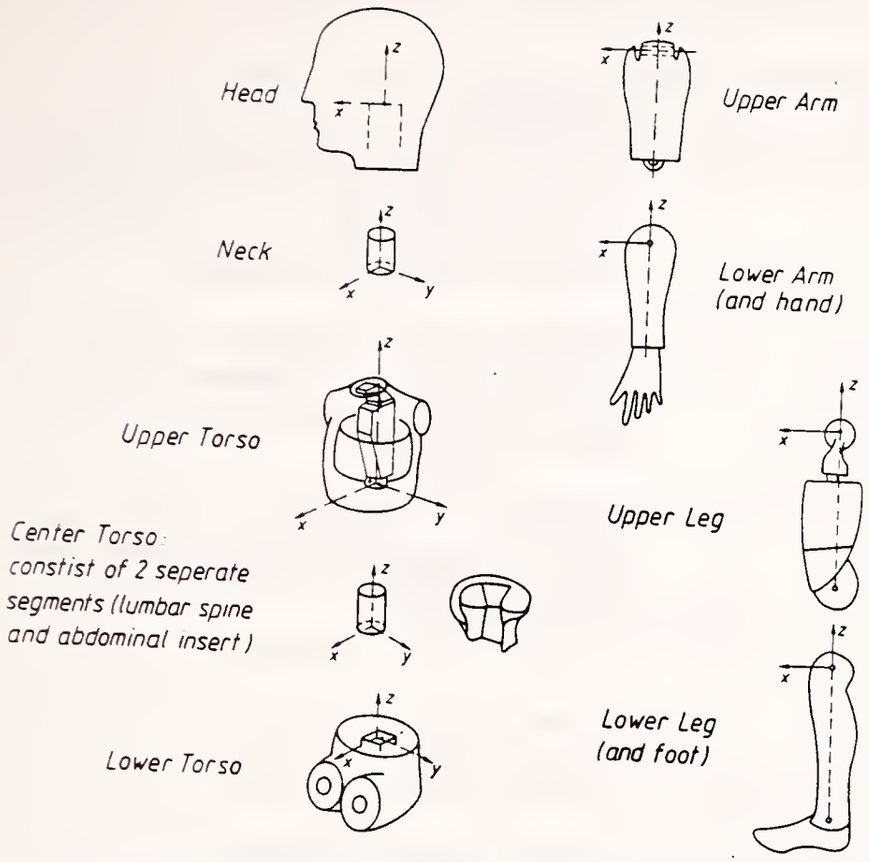

Figure 1

Division in segments and location of local coordinate systems

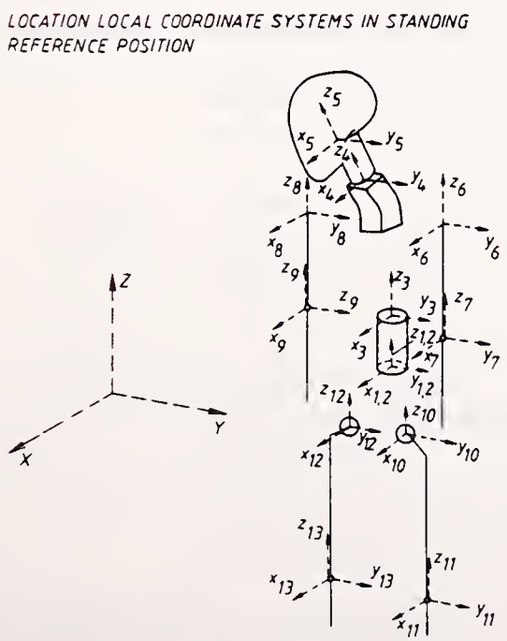

Figure 2

Location local coordinate systems in standing reference position

Table 1 Division of Part 572 Dummy in 13 Segments

NAME	COMMENTS
lower torso	CALSPAN: abdominal insert, lumbar spine and femur and retainer assembly E05/E06 are incorporated in the lower torso segment
center torso	Consists of 2 separate segments: lumbar spine and abdominal insert. Data for both components will be given separately.
upper torso	Includes shoulder. TNO and Hubbard: separate measurements for the shoulder.
neck	
head	
left (right) upper arm	
left (right) lower arm and hand	Hubbard: separate measurements for the hand and lower arm.
left (right) upper leg	CALSPAN: without femur and retainer assembly E05/E06.
left (right) lower leg and foot	Hubbard and CALSPAN: separate measurements for lower leg and foot.

Table 2 Specification of local coordinate system* (see Figure 1)

NAME	COMMENTS	
lower torso/central torso	origin:	centerline of lumbar spine at spine/lower torso attachment surface.
	z-axis:	along centerline lumbar spine
upper torso	origin:	centerline of lumbar spine at spine/upper torso attachment surface (i.e. in plane of bottom side of D/03 lumbar adapter).
	z-axis:	along centerline lumbar spine.
neck	origin:	centerline of neck at upper torso/neck attachment surface.
	z-axis:	along centerline neck.
head	origin:	centerline of neck at head/neck attachment surface.
	z-axis:	along centerline neck.
upper arm	origin:	center of shoulder pivot for abduction/adduction motions.
	x-axis:	along centerline of shoulder pivot for abduction/adduction motions.
	z-axis:	along the line between center of shoulder and elbow pivot.
lower arm	origin:	center of elbow pivot.
	y-axis:	along centerline of elbow
	z-axis:	along the line between the pivot center of the elbow and the center of the wrist pivot.
upper leg	origin:	center of the hip.
	y-axis:	parallel to centerline of knee-pivot bolt.
	z-axis:	intersects the knee centerline.
lower leg	origin:	center of knee.
	y-axis:	along the centerline of the knee pivot bolt.
	z-axis:	along a line from the center of the ankle joint (flexion joint) to the center of the knee joint.

* Note: if not specified in another way, all positive z-axis are upward, all positive x-axis are forward and all positive y-axis are to the left (in standing position).

Table 3 Segment Masses

NAME	SIERRA HUBBARD (kg)	HUBBARD (kg)	ALDERSON CALSPAN (kg)	TNO (kg)
lower torso	12.7	11.6	11.62[1)]	11.1
lumbar spine	1.4	1.29	1.36	1.33
abdominal insert	1.2	1.4	1.44	1.32
upper torso[2)]	17.4	17.7	17.16	17.18
neck	0.9	0.9	0.82	0.89
head	4.5	4.6	4.38	4.2
one upper arm	2.2	2.2	2.16	2.3
one lower arm & one hand	2.15	2.2	2.09	2.16
one upper leg	9.9	9.85	9.55[3)]	9.41
one lower leg & one foot	4.4	4.3	4.42	4.54
total dummy mass[4)]	75.4	74.59	73.22	72.84

1) After correction for mass abdominal insert (- 1.44 kg), lumbar spine (- 1.36 kg), and femur and retainer assembly (- 1.4 kg).
2) Includes shoulders (mass of one shoulder is 1.6 kg (Alderson) and 1.5 kg (Sierra) according to Hubbard measurements and 1.45 kg according to TNO measurements).
3) After correction for mass of femur and retainer assembly (+ 1.4 kg)
4) Sum of separate segments.

Table 4

Center of Gravity

locations: x, y and z coordinates (in mm) with respect to local coordinate systems[1)]

Name	SIERRA Hubbard x	SIERRA Hubbard y	SIERRA Hubbard z	ALDERSON Hubbard x	ALDERSON Hubbard y	ALDERSON Hubbard z	ALDERSON CALSPAN x	ALDERSON CALSPAN y	ALDERSON CALSPAN z	ALDERSON TNO x	ALDERSON TNO y	ALDERSON TNO z
lower torso	30	0	- 78	26	0	- 77	46[5)]	0	- 40[5)]	21	0	- 62
lumbar spine[3)]	0	0	67	0	0	68	0	0	65[2)]	0	0	66[2)]
abdominal insert[3)]	57	0	83	57	0	72	--	--	--	66	0	60
upper torso	26	0	167	31	0	167	29	0	160	26[4)]	0	155[4)]
neck	0	0	62	0	0	63	0	0	62	0	0	63
head	8	0	25	2	0	29	9	0	29	--[6)]	0	--[6)]
upper arm[7)]	0	0	-126	0	0	-120	0	0	-119	0	0	-123
lower arm & hand[7)]	0	0	-176[8)]	0	0	-159[8)]	0	0	-161	0	0	-170
(left) upper leg[7)]	0	6	-206	0	0	-212	0	0	-240[9)]	0	11	-203
lower leg & foot[7)]	14[10)]	0	-276[10)]	19[10)]	0	-278[10)]	16[10)]	0	-265[10)]	16	0	-269

1) Values between -5 and +5 mm are neglected here.
2) Calculated.
3) Coordinate system of lumbar spine and abdominal insert are identical.
4) Calculated from separate measurements of torso and shoulder.
5) Includes here lumbar spine, abdomen and femur and retainer assembly EO5/EO6.
6) Measurement error.
7) Hubbard and TNO: average of left and right segment; CALSPAN: based on measurements of right segment.
8) Calculated from separate measurements of lower arm and hand.
9) Without femur and retainer assembly EO5/EO6.
10) Calculated from separate measurements of lower leg and foot.

Table 5

Segment principal moments of inertia with respect to center of gravity[1)]

Segment Name	SIERRA Hubbard Iy kgm^2	Hubbard Iy kgm^2	Ix kgm^2	CALSPAN Iy kgm^2	ALOERSON Iz kgm^2	Ix kgm^2	TNO Iy kgm^2	Iz kgm^2
lower torso	0.0800	0.0734	0.2245[4)]	0.1564[4)]	0.1673[4)]	0.1297	0.0901	0.1393
lumbar spine[5)]	0.0037	0.0036	0.0024	0.0024	0.0010	0.0024	0.0024	0.0009
abdominal insert	0.0087	0.0099	-----[3)]	-----[3)]	-----[3)]	0.0114	0.0096	0.0147
upper torso	0.1931	0.1958	0.2352	0.1799	0.1508	0.1949[6)]	0.1976[6)]	0.1220[6)]
neck[5)]	0.0019	0.0020	0.0013	0.0013	0.0006	0.0015	0.0015	0.0006
head	0.0301	0.0301	0.0248[7)]	0.0291	0.0184[7)]	0.0213	0.0333	0.0162
upper arm[9)]	0.0148	0.0154	0.0156	0.0161	0.0014	0.0165	0.0161	0.0018[8)]
lower arm & hand[9)]	------[12)]	------[12)]	0.0308	0.0292	0.0014	0.0314	0.0310	0.0013[8)]
upper leg[9)]	0.1445	0.1380	0.0875[10)]	0.0872[10)]	0.0130[10)]	0.1300	0.1336	0.0170
lower leg & foot[9)]	0.1266[11)]	0.1168[11)]	-----[2)]	-----[2)]	-----[2)]	0.1315	0.1380	0.0046[8)]

1) In both the Hubbard and TNO measurements, principal axis are assumed to have the same orientation as the local coordinate system.
2) Error in foot measurements.
3) Incorporated in lower torso.
4) Lower torso segment in these measurements include: abdomen, lumbar spine and femur and retainer assembly E05/E06. Principal axis x and z are rotated -23.62 degrees (backward) with respect to segment coordinate system.
5) Calculated in CALSPAN and TNO.
6) Lower torso segment in these measurement is without shoulder.
7) Principal axis rotated -42.64 degrees (backward) with respect to segment coordinate system.
8) Calculated.
9) Average of left and right segments (Hubbard and TNO); right segment (CALSPAN).
10) Without femur and retainer assembly E05/E06.
11) Calculated from separate measurements of foot and lower leg.
12) Arm and hand were separately measured.

Table 6
Relative positions (in mm) of coordinate systems (i.e. joint locations)[1)]

Joint Name	Relative to coordinate system of:	SIERRA			Hubbard			ALDERSON: CALSPAN[2)]			TNO[3)]		
		x	y	z	x	y	z	x	y	z	x	y	z
lower spine[4)]	lower torso	0	0	0	0	0	0	0	0	0	0	0	0
upper spine	center torso	0	0	132	0	0	132	0	0	131	0	0	131
lower neck	upper torso	65	0	315	63	0	317	67	0	321	67	0	322
upper neck[5)]	neck	0	0	124	0	0	125	0	0	124	0	0	125
(left) shoulder[6)]	upper torso	29	189	272	36	190	263	25	188	245	31	188	250
elbow[6)]	upper arm	0	0	-258	0	0	-262	0	0	-262	0	0	-281
(left) hip[6)]	lower torso	--[7)]	--[7)]	--[7)]	--[7)]	--[7)]	--[7)]	42	87	- 72	65	66	- 75
(left) knee[6)]	upper leg	0	6	-400	0	5	-402	0	13	-412	0	9	-390

1) In this table, positions of the origin of a coordinate system are expressed in the coordinate system of another adjoining segment, values less than 5 mm are taken zero.
2) In the CALSPAN CVS model, pivots for simulation of the neck and the spine are not located in the end points of the cylinders. Consequently, they don't coincide with the origin of a segment coordinate system.
3) These TNO data were estimated from assembly drawings rather than based on measurements and, consequently, they are considered to be less accurate.
4) All values are zero here since center torso and lower torso segments have identical origins.
5) The neck (and the neck coordinate system) is pitched +20 degrees (forward) relative to the upper torso.
6) TNO and Hubbard: average of right and left segments; CALSPAN: measurement of right segment. Coordinates presented in the coordinate system of a left segment
7) Not measured.

Table 7 Model Dataset: Masses and Moments of Inertia[1)]

NAME	MASS[2)]	Moments of Inertia		
	kg	Ix kgm^2	Iy kgm^2	Iz kgm^2
lower torso	11.76	0.1297[3)]	0.0817[6)]	0.1393[3)]
center torso	2.69	0.0140[3)]	0.0159[6)]	0.0186[3)]
upper torso	17.36	0.2352[4)]	0.1896[7)]	0.1508[4)]
neck	0.88	0.0014[5)]	0.0014[5)]	0.0006[5)]
head	4.42	0.0248[4)]	0.0307[2)]	0.0184[4)]
upper arm	2.22	0.0161[5)]	0.0156[2)]	0.0016[5)]
lower arm	2.15	0.0311[5)]	0.0301[5)]	0.0014[5)]
upper leg	9.68	0.1300[3)]	0.1387[6)]	0.0170[3)]
lower leg	4.42	0.1315[3)]	0.1271[6)]	0.0046[3)]
total dummy mass	74.05			

1) Except for the head, orientation of principal axes is taken identical to local coordinate axes. For the head, the principal axis system is taken -43 degrees rotated about the y-axis of the local head coordinate system (i.e. rotated backward).
2) Average Hubbard/CALSPAN/TNO
3) TNO
4) CALSPAN
5) Average CALSPAN/TNO
6) Average Hubbard/TNO
7) Average Hubbard/CALSPAN.

Table 8 Model Dataset: Location Center of Gravity

NAME	x (M)	y (M)	z (M)
lower torso[1]	0.026	0	-0.079
center torso[3]	0.033	0	0.072
upper torso[2]	0.029	0	0.162
neck[2]	0	0	0.063
head[4]	0.006	0	0.028
upper arm[2]	0	0	-0.122
lower arm[2]	0	0	-0.167
(left) upper leg[1]	0	0.006	-0.207
lower leg[2]	0.016	0	-0.272

1) Average of Hubbard/TNO
2) Average of Hubbard/CALSPAN/TNO
3) Calculated from lumbar spine and abdominal insert values of Hubbard/TNO
4) Average of Hubbard/CALSPAN.

Table 9 Model Dataset: Location Origin of Joints

NAME	Relative to coordinate system of:	x (m)	y (m)	z (m)
lower spine	lower torso	0	0	0
upper spine[1]	center torso	0	0	0.132
lower neck[1]	upper torso	0.065	0	0.318
upper neck[1]	neck	0	0	0.124
(left) shoulder[1]	upper torso	0.030	0.189	0.260
elbow[1]	upper arm	0	0	-0.261
(left) hip[2]	lower torso	0.042	0.087	-0.072
(left) knee[1]	upper leg	0	0.008	-0.405

1) Average of Hubbard/Calspan
2) Calspan.

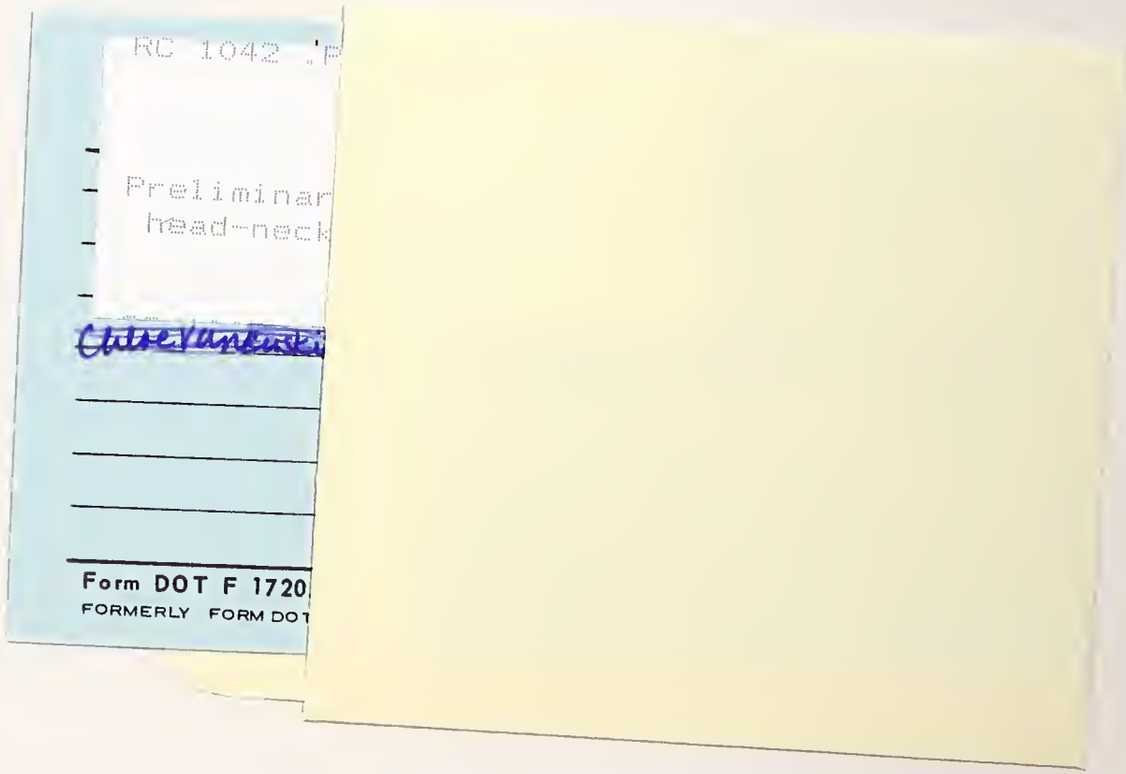
RC 1042 .P
Preliminar
head-neck
Form DOT F 1720
FORMERLY FORM DOT